Table 2. Change in Free Energy (kcal/mol) Associated with D30N Mutation[a]

inhibitor	$\Delta\Delta G_{qm/wat}$ (kcal/mol)	$\Delta\Delta G_{mm/wat}$ (kcal/mol)	$\Delta\Delta G_{qm}$ (kcal/mol)	$\Delta\Delta G_{mm}$ (kcal/mol)	IC_{50} fold change[b]
saquinavir	+4	+4	−1	−2	3.9
nelfinavir	+7	+9	−11	−9	5.3
lopinavir	n.d.	n.d.	+17	+21	3.1
amprenavir	−12	+12	+11	+7	0.2
tipranavir	−5	−2	−12	−9	0.03

[a] The qm subscript refers to the use of protein-polarized QM charges on the inhibitor, and the mm subscript refers to the use of fixed force-field-based charges. The use of an explicit bridging water is shown by the wat subscript. A positive $\Delta\Delta G$ indicates a decrease in binding affinity, while a negative $\Delta\Delta G$ indicates an increase. [b] IC_{50} fold change greater than 1 indicates a reduction in potency with D30N mutation, while a fold change of less than 1 indicates sensitivity.

Table 3. Correlation Coefficient (r) of the Free Energies of Binding versus Experimental IC_{50} Data[a]

	Set-1 (PRO^{WT},PRO^{D30N},PRO^{I50V})				Set-2 (PRO^{WT},PRO^{D30N},PRO^{I50V},$PRO^{V82I/I85V}$)				Set-3 (PRO^{WT} and all mutant proteases)			
	r_{mm}	r_{qm}	$r_{mm/wat}$	$r_{qm/wat}$	r_{mm}	r_{qm}	$r_{mm/wat}$	$r_{qm/wat}$	r_{mm}	r_{qm}	$r_{mm/wat}$	$r_{qm/wat}$
DRV	0.30	**0.91**	**0.93**	**0.93**	0.14	**0.65**	**0.53**	**0.81**	0.29	0.23	0.46	**0.83**
98065	0.35	0.18	**0.99**	**0.94**	0.31	0.40	0.32	**0.66**	**0.53**	0.17	0.46	0.48
APV	0.26	**0.66**	**0.57**	**0.99**	0.34	0.23	0.47	**0.88**	0.31	0.19	0.29	**0.60**
02031	0.16	**0.78**	0.24	**0.78**	0.46	0.48	0.21	0.10	0.61	**0.62**	0.02	0.19
TPV	**0.96**	**0.70**	0.49	**0.83**	**0.91**	**0.71**	0.01	**0.68**	0.14	0.04	0.04	**0.50**
NFV	0.21	**0.51**	**0.83**	**0.77**	0.26	0.35	**0.71**	**0.59**	0.11	0.31	0.41	0.39
NFV	0.21	**0.51**	**0.62**[b]	**0.97**[b]	0.26	0.35	0.48[b]	**0.92**[b]	0.11	0.31	0.18[b]	**0.58**[b]
LPV	**0.76**	**0.97**	n.d.	n.d.	0.42	**0.59**	n.d.	n.d.	0.16	**0.66**	n.d.	n.d.
SQV	0.06	0.45	**0.96**	**0.99**	0.11	0.43	**0.94**	**0.87**	**0.78**	0.22	**0.57**	**0.84**
AZV	**0.76**	**0.54**	0.06	0.16	0.13	0.14	0.35	0.16	0.24	0.17	**0.66**	**0.59**
AZV	**0.76**	**0.54**	**0.91**[b]	**0.64**[b]	0.13	0.14	0.34[b]	**0.53**[b]	0.24	0.17	**0.62**[b]	**0.58**[b]

[a] The qm subscript refers to the use of protein-polarized QM charges on the inhibitor, and the mm subscript refers to the use of fixed force-field-based charges. The use of an explicit bridging water is shown by the wat subscript. Bold font indicates correlation ($r > 0.5$). [b] Calculated with three water molecules that mediate hydrogen bonds between the protease and the inhibitor.

was resistant to NFV by 5.3-fold compared to HIV^{WT}, and $\Delta\Delta G_{qm/wat}$ showed an increase in the free energy of binding by +7 kcal/mol. HIV-1 containing PRO^{D30N} was more sensitive to APV and TPV, and $\Delta\Delta G_{qm/wat}$ for PRO^{D30N} with APV and TPV was −12 and −5 kcal/mol, respectively (Table 2). The $\Delta\Delta G_{qm/wat}$ values showed that both TPV and APV had a higher affinity for PRO^{D30N} than for PRO^{WT} (Table 2) and correlated with the increase in sensitivity to these inhibitors.

We next compared the free energy changes ($\Delta\Delta G_{mm/wat}$) simulated using the bridging water molecule but with force-field-based fixed MM charges on the inhibitors. The $\Delta\Delta G_{mm/wat}$ values of +4 and +9 kcal/mol for SQV and NFV, respectively, showed that the simulation results in an increase in the free energy of binding correlating with the reduction of antiviral activity. However, the $\Delta\Delta G_{mm/wat}$ value showed a wrong trend for APV (+12 kcal/mol) and was alike for TPV (−2 kcal/mol). The $\Delta\Delta G_{qm}$ and $\Delta\Delta G_{mm}$ values were negative for SQV and NFV, respectively, while they were positive for APV. Thus, $\Delta\Delta G_{qm}$ and $\Delta\Delta G_{mm}$ values, which did not incorporate the bridging water molecule explicitly, simulated inaccurate changes in the free energy of binding for SQV, NFV, and APV. The crystal structure for LPV (PDB ID 1MUI) did not have any water molecules present, and all simulations involving LPV were carried out with implicit water. The $\Delta\Delta G_{qm}$ and $\Delta\Delta G_{mm}$ values for LPV were +17 and +21 kcal/mol, respectively. The increase in the change in the free energy of binding of LPV with PRO^{D30N} was consistent with its decrease in antiviral potency with D30N substitution. For TPV, the negative $\Delta\Delta G_{qm}$ and $\Delta\Delta G_{mm}$ values indicated favorable free energy of binding for PRO^{D30N} compared to PRO^{WT} and correlated with the increase in antiviral potency of TPV with the D30N mutant.

In summary, the $\Delta\Delta G_{qm/wat}$ values provided consistent trends of the change in free energy of binding for PRO^{D30N}, which is resistant to SQV and NFV but is more sensitive to APV and TPV. $\Delta\Delta G_{qm}$ and $\Delta\Delta G_{mm}$ did not always provide the correct trend of change in the free energies of binding.

Correlation of Free Energy and Antiviral Potency for Active Site Mutants. The GBSA free energies were simulated under four conditions: (i) with implicit solvation terms and MM charges on both ligand and protein (ΔG_{mm}), (ii) with explicit water and implicit solvation terms (hybrid solvation model) with MM charges on both ligand and protein ($\Delta G_{mm/wat}$), (iii) with implicit solvation terms and protein-polarized QM charges on the ligand and MM charges on the protein (ΔG_{qm}), and (iv) with explicit water and implicit solvation terms (hybrid solvation model) with QM charges on the ligand and MM charges on the protein ($\Delta G_{qm/wat}$). All the free energy values determined are shown in Supporting Information Tables S1 and S2.

We analyzed the correlation of the free energies thus computed with the experimentally determined antiviral potency data (IC_{50}), and the resultant correlation coefficients are shown in Table 3, where Set-1 refers to the correlation coefficient for PRO^{WT}, PRO^{D30N}, and PRO^{I50V}, Set-2 refers to the correlation coefficient for PRO^{WT}, PRO^{D30N}, PRO^{I50V}, and $PRO^{V82I/I85V}$, and Set-3 refers to the correlation coefficients for PRO^{WT}, PRO^{D30N}, PRO^{I50V}, $PRO^{V82I/I85V}$, PRO^{2840}, and PRO^{2841}. For Set-1, r_{mm} (correlation coefficient of ΔG_{mm} vs IC_{50}) showed a strong correlation for only TPV, LPV, and AZV (Table 3). The r_{mm} value was poor for the other PIs and indicates the difficulty of obtaining reasonable

correlations between free energies and antiviral potency. The r_{qm} (correlation coefficient of ΔG_{qm} vs IC_{50}) values that represented correlation coefficients when the free energies were simulated with polarized QM charges on the ligands showed significant improvement and a strong correlation for DRV, APV, GRL-02031, and LPV. However, both r_{mm} and r_{qm} values were poor for GRL-98065 and SQV.

We next determined, for Set-1, the correlation obtained by the hybrid water model that has an explicit bridging water molecule between the inhibitor and the protease flap. The explicit water was treated as a part of the protein, and implicit solvation terms were used. The $r_{mm/wat}$ value (correlation coefficient of $\Delta G_{mm/wat}$ vs IC_{50}) represented a greater correlation than r_{mm} for all PIs except TPV and AZV. TPV directly formed hydrogen bonds with Ile50 and Ile50′, and the water molecule included in this calculation formed hydrogen bonds with Gly48 of one monomer of the protease dimer. For other PIs, the bridging water molecule formed hydrogen bonds with the flaps from both monomers. The $r_{qm/wat}$ value (correlation coefficient of $\Delta G_{qm/wat}$ vs IC_{50}) had a high degree of correlation for all PIs except AZV. Thus, the explicit inclusion of the water molecule bridging hydrogen bonds with the flap and protein-polarized QM charges for the inhibitors provided strong correlation ($r > 0.75$) for seven out of eight inhibitors. The correlation coefficient $r_{qm/wat}$ for NFV with three bridging waters was 0.97, a significant improvement over the correlation coefficient of 0.77 obtained with one bridging water molecule. The $r_{qm/wat}$ value for AZV also improved from 0.16 to 0.64 with the inclusion of three bridging water molecules.

We also determined r_{mm}, r_{qm}, $r_{mm/wat}$, and $r_{qm/wat}$ values for Set-2, which included $PRO^{V82I/I85V}$ as well (Table 3). The r_{mm} value was poor for all PIs except TPV, while the r_{qm} values showed good correlations for DRV, LPV, and TPV. The $r_{mm/wat}$ value showed strong correlation for only SQV and good correlation ($0.55 < r < 0.75$) for NFV. The $r_{qm/wat}$ value showed strong correlations for DRV, APV, and SQV and good correlations for GRL-98065 and TPV. The $r_{qm/wat}$ value for NFV jumped from 0.59 to 0.92 with the incorporation of three bridging water molecules instead of one.

The correlation coefficients with a hybrid water model and with QM-polarized ligand charges ($r_{qm/wat}$) on the PIs were higher for most of the PIs compared to the correlation coefficients obtained without any explicit water molecule and MM charges (r_{mm}). The only exception was for TPV, which was the only nonpeptidomimetic inhibitor among the PIs examined. TPV displaces the tetracoordinated water molecule and interacts directly with Ile50 and Ile50′ in the flap.[46] The hydrogen-bond interaction of the bridging water molecule with TPV and Gly48 of one chain might not be an important contributor to its potency. Also, in general, the $r_{qm/wat}$ values provided better correlations than r_{qm}.

Correlation of Free Energy and Antiviral Potency for Active and Nonactive Site Amino Acid Substitutions. We next analyzed the correlations of the free energies with the antiviral potency (IC_{50} values) for PRO^{WT}, PRO^{D30N}, PRO^{I50V}, $PRO^{V82I/I85V}$, PRO^{2840} that contains L10R, M46I, L63P, V82T, and I84V, and PRO^{2841} that contains M46I, L63P, V82T, and I84V substitutions (Set-3 in Table 3). The analysis of PRO^{2840} and PRO^{2841} was substantially complex since both proteases contained nonactive site substitutions, but it was worth examining the ability of the

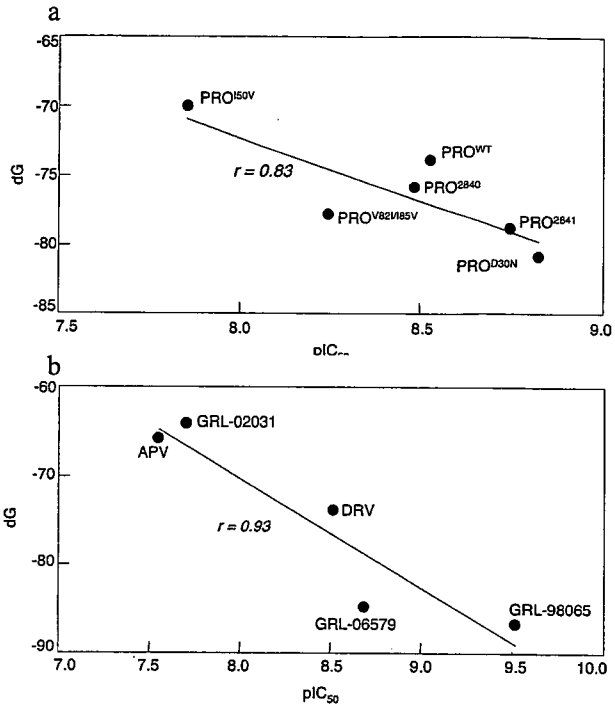

Figure 3. Correlation of free energy and antiviral activity. (a) Scatter plot of $\Delta G_{qm/wat}$ vs pIC_{50} for DRV for Set-3. (b) Scatter plot of $\Delta G_{qm/wat}$ vs pIC_{50} (PRO^{WT}) for ligands with bis-THF-related cores. The correlation coefficient is shown in both figures.

GBSA energy function to correlate with antiviral activity when substitutions distant from the inhibitor were present. In general, the correlation coefficients for Set-3 turned out to be low, indicating a lower correlation between the free energies and antiviral potencies when nonactive site mutants were present. For DRV, the r_{mm}, r_{qm}, and $r_{mm/wat}$ values indicated that the corresponding free energies had no correlation with IC_{50} values. However, the value of $r_{qm/wat}$ for DRV was 0.83, showing a strong correlation for simulations with polarized QM charges on the inhibitor with a hybrid water model (Table 3, Figure 3a). For SQV, strong correlations were obtained for both ΔG_{mm} with IC_{50} ($r_{mm} = 0.78$) and $\Delta G_{qm/wat}$ with IC_{50} ($r_{qm/wat} = 0.84$). For APV and TPV, $r_{qm/wat}$ values were 0.60 and 0.50, respectively, but there was no correlation when other GBSA protocols were used for these inhibitors. The $r_{qm/wat}$ values were greater than 0.75 for two inhibitors and greater than 0.55 for five inhibitors. The r_{qm} and $r_{mm/wat}$ values were greater than 0.55 for two inhibitors. Thus, the hybrid water model and inclusion of polarization effects, compared to the other protocols, simulated free energies with better correlation with antiviral IC_{50} for more inhibitors.

GBSA with Hybrid Water Model and Polarizable Quantum Charges on PIs as a Lead Optimization Tool. Obtaining a correct relative rank of activity for inhibitors that had potency in the nanomolar range has been a real challenge for scoring methods.[3] Scoring methods providing sufficiently high correlation with potency may serve as a lead optimization tool. In our data set, DRV and GRL-98065 have a bis-THF group as the core, GRL-06579 and GRL-02031 have a Cp-THF as the core, and APV has a THF group as the core. All these inhibitors were extremely potent against PRO^{WT} and had a narrow range of activity

Table 4. Experimental Free Energies[a] of Protease Inhibitors Against PRO^{WT}

	DRV	APV	GRL-98065	GRL-02031	GRL-06579
IC_{50} (μM)	0.003	0.028	0.0003	0.02	0.002
ΔG_{exp} (kcal/mol)	−11.6	−10.3	−13.0	−10.5	−11.9

[a] Experimental free energies determined as $\Delta G_{exp} = RT \ln(IC_{50})$, where R and T represent the universal gas constant and temperature, respectively.

ranging from 0.3 to 28 nM (Table 1). We computed ΔG_{exp} from the antiviral IC_{50} values (Table 4). Such transformations have recently enhanced the understanding of the binding of *N*-sulphonyl-glutamic acid inhibitors to MurD ligase and in understanding the efficiency of DNA catalysis.[19,47] Substitution of the THF group of APV with the bis-THF group (DRV) resulted in a −1.3 kcal/mol improvement in the free energy of binding. GRL-98065 has a 1,3-benzodioxole group as P2′ ligand compared to an aniline group in DRV, which resulted in the ΔG_{exp} of GRL-98065 being lower (i.e., better binding affinity) by −1.4 kcal/mol than DRV. Both GRL-06579 and GRL-02031 have a Cp-THF as the P2 ligand but different substituents interacting with the S1′ and S2′ locations in the protease active site. The ΔG_{exp} of GRL-06579 is lower by 1.4 kcal/mol than GRL-02031. Among these five PIs, APV and GRL-02031 have the worst ΔG_{exp} and GRL-98065 has the best ΔG_{exp}. The absolute magnitudes of our simulated GBSA free energies are larger than those measured experimentally due to the force-field parameters and the form of the energy function, but trends and correlation with experiments can be deduced. Our $\Delta G_{qm/wat}$ values simulated the correct trend by predicting that the worst binding free energy was for APV and GRL-02031, and the best binding free energy was for GRL-98065 (Supporting Information Table S1). None of the other GBSA protocols predicted the trend correctly (Supporting Information Tables S1 and S2). We further analyzed the correlation of the free energies calculated by our methods against IC_{50} values for these five PIs. The r_{mm} and $r_{mm/wat}$ values were 0.10 and 0.03, respectively, indicating that there was no correlation of GBSA free energies simulated by using MM charges with or without explicit inclusion of water. The difficulty of obtaining good correlation of free energies against antiviral activity is evident from this small but nontrivial data set. The r_{qm} value was 0.74, indicating that incorporation of protein-polarized QM charges on the inhibitors substantially improved the correlation. Including the bridging water molecule with protein-polarized QM charges on the PIs resulted in a $r_{qm/wat}$ value of 0.93 for PRO^{WT} (Figure 3b). Thus, a simulation using the hybrid water model and protein-polarized QM charges on the ligands resulted in a strong correlation, while there was no correlation for simulations with fixed MM charges.

For our docking and subsequent GBSA simulations, we used the crystal coordinates of BCV−protease complex (PDB ID 2FDE)[22] as our starting template. BCV, DRV, and GRL-98065 had a bis-THF moiety as the core ligand, and APV, GRL-06579, and GRL-02031 had cores that had a high similarity with bis-THF. The high correlation obtained with $\Delta G_{qm/wat}$-IC_{50} indicated that free energies obtained with a hybrid water model and polarized QM charges on the ligands would be a promising approach for lead optimization. Currently, we are exploring the utility of GBSA free energy simulations once a correct binding mode is obtained, and we wanted to use native or native-like crystal structure as a template as a proof-of-principle study. We have not explored docking ligands against non-native protease crystal structures in the current study. A more exhaustive examination that includes poses obtained by cross docking needs to be performed.

DISCUSSION

Progress has been made in improving the robustness of scoring functions to determine the relative affinity of inhibitors for target proteins, but there are vast scopes where significant improvement can be made.[1,3] Part of the reason for the inaccuracies in the scoring functions arise because (i) the current methodologies largely account for enthalpic changes while completely ignoring entropic changes, (ii) they do not properly treat protein flexibility, (iii) they do not properly account for solvation and desolvation effects, and (iv) they do not account for the polarization induced by the protein and the ligand on each other.[1,3,7] Most of the studies on scoring functions deal with rank ordering the activity of a congeneric set of ligands. The prediction of activity of a ligand against mutant proteins is very important in light of drug-resistance mutations that emerge in many therapeutic areas.

We explored the correlation of GBSA free energies with antiviral potency (IC_{50} values) of nine different PIs against wild-type and mutant proteases. Correlation with enzymatic K_i would result in similar conclusions since these PIs have good cell penetration and are highly protease-specific inhibitors. Furthermore, these PIs do not form aggregates and do not have the problematic properties discussed by Shoichet et al.[48,49]

The GBSA free energies were simulated by four different protocols: (i) fixed MM charges in implicit solvent (ΔG_{mm}), (ii) protein-polarized QM charges of PIs in implicit solvent (ΔG_{qm}), (iii) fixed MM charges in a hybrid solvent ($\Delta G_{mm/wat}$), and (iv) protein-polarized QM charges of PIs in a hybrid solvent ($\Delta G_{qm/wat}$). The hybrid solvent protocols have retained an explicit water molecule(s) that bridges hydrogen bonding with the protease in an otherwise implicit solvent environment. The protein-polarized ligand charges were determined during ligand docking in the protein environment at the B3LYP/6-31G* level, and these polarized charges were maintained for the ligand for the full GBSA simulation cycle. These enable us to analyze the effect of a different charge model compared to the static charges from a force field (Supporting Information Figures S3 and S4). Free energies from a successful GBSA protocol should provide a good correlation with the antiviral activity against wild-type and mutant protease. Resistance mutations in the protease active site arise primarily due to loss of favorable binding interactions. Resistance caused by nonactive site mutations is more difficult to understand and rationalize,

although some attempts to elucidate the mechanism have recently been made.[12,50−52]

We initially compared the correlation coefficients for PRO^{WT}, PRO^{D30N}, and PRO^{I50V} (Set-1). The antiviral potency of the inhibitors for wild-type and mutant proteases are shown in Table 1, and the inhibitors have potency (IC_{50} values) in the nanomolar range. The $r_{qm/wat}$ value was higher than 0.75 for 7 out of 8 PIs for Set-1, with $r_{qm/wat}$ being more than 0.90 for 4 PIs (Table 3). PRO^{D30N} was associated with SQV, NFV, and LPV resistance of HIV-1 and increased susceptibility to APV and TPV (Table 1). It is noteworthy that $r_{qm/wat}$ showed substantial correlation values of greater than 0.75 even though the fold change in antiviral activity for PRO^{D30N} is nonmonotonic. AZV is the only PI that did not show a correlation of $\Delta G_{qm/wat}$ with the IC_{50} value with one bridging water molecule. By including two additional bridging water molecules for NFV and AZV, $r_{qm/wat}$ improved to 0.97 and 0.64, respectively. Selective inclusion of explicit water molecules needs to be explored and validated. For Set-1, $r_{mm/wat}$, r_{qm}, and r_{mm} had strong correlation for 4, 3, and 3 PIs, respectively.

Correlations for Set-2 included the mutant $PRO^{V82I/I85V}$. While V82I is located in the protease active site and represents one of the major resistance-associated mutations for PIs, I85V was selected as a resistance-associated mutation for GRL-98065 even though it does not form a direct van der Waals contact.[32] For Set-2, the number of PIs that showed strong correlation coefficients for $r_{qm/wat}$ and $r_{mm/wat}$ were 4 and 1, respectively, while r_{qm} and r_{mm} did not show strong correlations for any PI. Set-3 included Set-2 as well as PRO^{2840} and PRO^{284J}, which had mutations distant from the active site. We included such mutations because they are seen in drug-resistant HIV-1-harboring patients, and we wanted to test the ability of the GBSA energy function to correlate with the antiviral IC_{50} for such protease substitutions. The $r_{qm/wat}$ values showed strong correlation coefficients for only DRV and SQV for Set-3 and moderate correlation for 3 other PIs. The correlation coefficients, $r_{mm/wat}$ and r_{qm}, were from 0.55 to 0.75 for two PIs in Set-3, suggesting that those two PIs had a moderate correlation between the free energies and the IC_{50} values.

Analysis of correlation coefficients in Table 3 indicated that $r_{qm/wat}$ had strong ($r > 0.75$) and moderate ($0.55 < r < 0.75$) correlation for more PIs than $r_{mm/wat}$, r_{qm}, or r_{mm}. This suggested that the GBSA free energies simulated with a hybrid water model with protein-polarized QM charges on the inhibitors had a higher correlation with antiviral IC_{50} than the other free energy simulation protocols. Others[1,3] have suggested that improved treatment of solvation and polarizability may improve the robustness of scoring functions, and we demonstrated that our use of selected explicit water molecule(s) and protein-polarized QM partial charges on the inhibitor provided greater correlation with antiviral potency. Further improvement might be achieved by (i) improving upon the hybrid water model (ii) by accounting for the polarization induced by the inhibitors on the protein atoms and (iii) by including changes in entropy.

ACKNOWLEDGMENT

This work was supported in part by the Intramural Research Program of the Center for Cancer Research, National Cancer Institute, National Institutes of Health (D.D. and H.M.), a grant from the National Institutes of Health (GM 53386 to A.K.G.), a grant from the Kumamoto University Global Center of Excellence Program, Global Education and Research Center Aiming at the control of AIDS (H.M.) supported by the Ministry of Education, Culture, Sports, Science, and Technology (Monbu-Kagakusho), a Grant-in-Aid for Scientific Research (Priority Areas to H.M.) from the Ministry of Education, Culture, Sports, Science, and Technology (Monbu-Kagakusho) of Japan (H.M.), and a Grant for Promotion of AIDS Research from the Ministry of Health, Labor and Welfare (Kosei-Rodosho) of Japan (H.M.). The work utilized the computational resources of the Biowulf cluster at the NIH.

Supporting Information Available: Simulated GBSA free energies; charges on DRV for OPLS2005 force field (MM level) and protein-polarized charges at the B3LYP/6-31G* level. This material is available free of charge via the Internet at http://pubs.acs.org.

REFERENCES AND NOTES

(1) Clark, D. E. What has virtual screening ever done for drug discovery. *Expert Opin. Drug Discovery* **2008**, *3*, 841–851.
(2) Lyne, P. D.; Lamb, M. L.; Saeh, J. C. Accurate prediction of the relative potencies of members of a series of kinase inhibitors using molecular docking and MM-GBSA scoring. *J. Med. Chem.* **2006**, *49*, 4805–4808.
(3) Leach, A. R.; Shoichet, B. K.; Peishoff, C. E. Prediction of protein-ligand interactions. Docking and scoring: Successes and gaps. *J. Med. Chem.* **2006**, *49*, 5851–5855.
(4) Rajamani, R.; Good, A. C. Ranking poses in structure-based lead discovery and optimization: Current trends in scoring function development. *Curr. Opin. Drug Discovery Dev.* **2007**, *10*, 308–315.
(5) Lu, Y. P.; Wang, R. X.; Yang, C. Y.; Wang, S. M. Analysis of ligand-bound water molecules in high-resolution crystal structures of protein-ligand complexes. *J. Chem. Inf. Model.* **2007**, *47*, 668–675.
(6) Huang, N.; Shoichet, B. K. Exploiting ordered waters in molecular docking. *J. Med. Chem.* **2008**, *51*, 4862–4865.
(7) Fornabaio, M.; Spyrakis, F.; Mozzarelli, A.; Cozzini, P.; Abraham, D. J.; Kellogg, G. E. Simple, intuitive calculations of free energy of binding for protein-ligand complexes. 3. The free energy contribution of structural water molecules in HIV-1 protease complexes. *J. Med. Chem.* **2004**, *47*, 4507–4516.
(8) Yin, P. D.; Das, D.; Mitsuya, H. Overcoming HIV drug resistance through rational drug design based on molecular, biochemical, and structural profiles of HIV resistance. *Cell. Mol. Life Sci.* **2006**, *63*, 1706–1724.
(9) Clemente, J. C.; Moose, R. E.; Hemrajani, R.; Whitford, L. R. S.; Govindasamy, L.; Reutzel, R.; McKenna, R.; Agbandje-McKenna, M.; Goodenow, M. M.; Dunn, B. M. Comparing the accumulation of active- and nonactive-site mutations in the HIV-1 protease. *Biochemistry* **2004**, *43*, 12141–12151.
(10) Hong, L.; Zhang, X. J. C.; Hartsuck, J. A.; Tang, J. Crystal structure of an in vivo HIV-1 protease mutant in complex with saquinavir: Insights into the mechanisms of drug resistance. *Protein Sci.* **2000**, *9*, 1898–1904.
(11) Kozisek, M.; Bray, J.; Rezacova, P.; Saskova, K.; Brynda, J.; Pokorna, J.; Mammano, F.; Rulisek, L.; Konvalinka, J. Molecular analysis of the HIV-1 resistance development: Enzymatic activities, crystal structures, and thermodynamics of nelfinavir-resistant HIV protease mutants. *J. Mol. Biol.* **2007**, *374*, 1005–1016.
(12) Mahalingam, B.; Wang, Y. F.; Boross, P. I.; Tozser, J.; Louis, J. M.; Harrison, R. W.; Weber, I. T. Crystal structures of HIV protease V82A and L90M mutants reveal changes in the indinavir-binding site. *Eur. J. Biochem.* **2004**, *271*, 1516–1524.
(13) Ghosh, A. K.; Sridhar, P. R.; Leshchenko, S.; Hussain, A. K.; Li, J. F.; Kovalevsky, A. Y.; Walters, D. E.; Wedekind, J. E.; Grum-Tokars, V.; Das, D.; Koh, Y.; Maeda, K.; Gatanaga, H.; Weber, I. T.; Mitsuya, H. Structure-based design of novel HIV-1 protease inhibitors to combat drug resistance. *J. Med. Chem.* **2006**, *49*, 5252–5261.
(14) Kovalevsky, A. Y.; Tie, Y. F.; Liu, F. L.; Boross, P. I.; Wang, Y. F.; Leshchenko, S.; Ghosh, A. K.; Harrison, R. W.; Weber, I. T.

Effectiveness of nonpeptide clinical inhibitor TMC-114 on HIV-1 protease with highly drug resistant mutations D30N, I50V, and L90M. *J. Med. Chem.* **2006**, *49*, 1379–1387.

(15) Tie, Y. F.; Kovalevsky, A. Y.; Boross, P.; Wang, Y. F.; Ghosh, A. K.; Tozser, J.; Harrison, R. W.; Weber, I. T. Atomic resolution crystal structures of HIV-1 protease and mutants V82A and I84V with saquinavir. *Proteins* **2007**, *67*, 232–242.

(16) Aqvist, J.; Medina, C.; Samuelsson, J. E. New Method for Predicting Binding-Affinity in Computer-Aided Drug Design. *Protein Eng.* **1994**, *7*, 385–391.

(17) Straatsma, T. P.; McCammon, J. A. Computational Alchemy. *Annu. Rev. Phys. Chem.* **1992**, *43*, 407–435.

(18) Bren, U.; Martinek, V.; Florian, J. Free energy simulations of uncatalyzed DNA replication fidelity: structure and stability of T.G and dTTP.G Terminal DNA mismatches flanked by a single dangling nucleotide. *J. Phys. Chem. B* **2006**, *110*, 10557–10566.

(19) Perdih, A.; Bren, U.; Solmajer, T. Binding free energy calculations of N-sulphonyl-glutamic acid inhibitors of MurD ligase. *J. Mol. Model.* **2009**, *15*, 983–996.

(20) Wang, Y. F.; Tie, Y. F.; Boross, P. I.; Tozser, J.; Ghosh, A. K.; Harrison, R. W.; Weber, I. T. Potent new antiviral compound shows similar inhibition and structural interactions with drug resistant mutants and wild type HIV-1 protease. *J. Med. Chem.* **2007**, *50*, 4509–4515.

(21) Vega, S.; Kang, L. W.; Velazquez-Campoy, A.; Kiso, Y.; Amzel, L. M.; Freire, E. A structural and thermodynamic escape mechanism from a drug resistant mutation of the HIV-1 protease. *Proteins* **2004**, *55*, 594–602.

(22) Miller, J. F.; Andrews, C. W.; Brieger, M.; Furfine, E. S.; Hale, M. R.; Hanlon, M. H.; Hazen, R. J.; Kaldor, I.; McLean, E. W.; Reynolds, D.; Sammond, D. M.; Spaltenstein, A.; Tung, R.; Turner, E. M.; Xu, R. X.; Sherrill, R. G. Ultra-potent P1 modified arylsulfonamide HIV protease inhibitors: The discovery of GW0385. *Bioorg. Med. Chem. Lett.* **2006**, *16*, 1788–1794.

(23) Krohn, A.; Redshaw, S.; Ritchie, J. C.; Graves, B. J.; Hatada, M. H. Novel Binding Mode of Highly Potent HIV-Proteinase Inhibitors Incorporating the (R)-Hydroxyethylamine Isostere. *J. Med. Chem.* **1991**, *34*, 3340–3342.

(24) Muzammil, S.; Armstrong, A. A.; Kang, L. W.; Jakalian, A.; Bonneau, P. R.; Schmelmer, V.; Amzel, L. M.; Freire, E. Unique thermodynamic response of tipranavir to human immunodeficiency virus type 1 protease drug resistance mutations. *J. Virol.* **2007**, *81*, 5144–5154.

(25) Kaldor, S. W.; Kalish, V. J.; Davies, J. F.; Shetty, B. V.; Fritz, J. E.; Appelt, K.; Burgess, J. A.; Campanale, K. M.; Chirgadze, N. Y.; Clawson, D. K.; Dressman, B. A.; Hatch, S. D.; Khalil, D. A.; Kosa, M. B.; Lubbehusen, P. P.; Muesing, M. A.; Patick, A. K.; Reich, S. H.; Su, K. S.; Tatlock, J. H. Viracept (nelfinavir mesylate, AG1343): A potent, orally bioavailable inhibitor of HIV-1 protease. *J. Med. Chem.* **1997**, *40*, 3979–3985.

(26) Stoll, V.; Qin, W. Y.; Stewart, K. D.; Jakob, C.; Park, C.; Walter, K.; Simmer, R. L.; Helfrich, R.; Bussiere, D.; Kao, J.; Kempf, D.; Sham, H. L.; Norbeck, D. W. X-ray crystallographic structure of ABT-378 (lopinavir) bound to HIV-1 protease. *Bioorg. Med. Chem.* **2002**, *10*, 2803–2806.

(27) Clemente, J. C.; Coman, R. M.; Thiaville, M. M.; Janka, L. K.; Jeung, J. A.; Nukoolkarn, S.; Govindasamy, L.; Agbandje-McKenna, M.; McKenna, R.; Leelamanit, W.; Goodenow, M. M.; Dunn, B. M. Analysis of HIV-1CRF_01 A/E protease inhibitor resistance: Structural determinants for maintaining sensitivity and developing resistance to atazanavir. *Biochemistry* **2006**, *45*, 5468–5477.

(28) Cho, A. E.; Guallar, V.; Berne, B. J.; Friesner, R. Importance of accurate charges in molecular docking: Quantum mechanical/molecular mechanical (QM/MM) approach. *J. Comput. Chem.* **2005**, *26*, 915–931.

(29) Friesner, R. A.; Banks, J. L.; Murphy, R. B.; Halgren, T. A.; Klicic, J. J.; Mainz, D. T.; Repasky, M. P.; Knoll, E. H.; Shelley, M.; Perry, J. K.; Shaw, D. E.; Francis, P.; Shenkin, P. S. Glide: a new approach for rapid, accurate docking and scoring. 1. Method and assessment of docking accuracy. *J. Med. Chem.* **2004**, *47*, 1739–49.

(30) Friesner, R. A.; Murphy, R. B.; Repasky, M. P.; Frye, L. L.; Greenwood, J. R.; Halgren, T. A.; Sanschagrin, P. C.; Mainz, D. T. Extra precision glide: docking and scoring incorporating a model of hydrophobic enclosure for protein-ligand complexes. *J. Med. Chem.* **2006**, *49*, 6177–96.

(31) Yu, Z. Y.; Jacobson, M. P.; Friesner, R. A. What role do surfaces play in GB models? A new-generation of surface-generalized Born model based on a novel Gaussian surface for biomolecules. *J. Comput. Chem.* **2006**, *27*, 72–89.

(32) Amano, M.; Koh, Y.; Das, D.; Li, J. F.; Leschenko, S.; Wang, Y. F.; Boross, P. I.; Weber, I. T.; Ghosh, A. K.; Mitsuya, H. A novel bis-tetrahydrofuranylurethane-containing nonpeptidic protease inhibitor (PI), GRL-98065, is potent against multiple-PI-resistant human immunodeficiency virus in vitro. *Antimicrob. Agents Chemother.* **2007**, *512*143–2155.

(33) Ghosh, A. K.; Leshchenko, S.; Noetzel, M. Stereoselective photochemical 1,3-dioxolane addition to 5-alkoxymethyl-2(5H)-furanone: Synthesis of bis-tetrahydrofuranyl ligand for HIV protease inhibitor UIC-94017 (TMC-114). *J. Org. Chem.* **2004**, *69*, 7822–7829.

(34) Ghosh, A. K.; Leshchenko-Yashchuk, S.; Anderson, D. D.; Baldridge, A.; Noetzel, M.; Miller, H. B.; Tie, Y. F.; Wang, Y. F.; Koh, Y.; Weber, I. T.; Mitsuya, H. Design of HIV-1 Protease Inhibitors with pyrrolidinones and oxazolidinones as novel P1′-Ligands To Enhance Backbone-Binding Interactions with Protease: Synthesis, Biological Evaluation, and Protein-Ligand X-ray Studies. *J. Med. Chem.* **2009**, *52*, 3902–3914.

(35) Koh, Y.; Das, D.; Leschenko, S.; Nakata, H.; Ogata-Aoki, H.; Amano, M.; Nakayama, M.; Ghosh, A. K.; Mitsuya, H. GRL-02031, a novel nonpeptidic protease inhibitor (PI) containing a stereochemically defined fused cyclopentanyltetrahydrofuran potent against multi-PI-resistant human immunodeficiency virus type 1 In Vitro. *Antimicrob. Agents Chemother.* **2009**, *53*, 997–1006.

(36) Yoshimura, K.; Kato, R.; Yusa, K.; Kavlick, M. F.; Maroun, V.; Nguyen, A.; Mimoto, T.; Ueno, T.; Shintani, M.; Falloon, J.; Masur, H.; Hayashi, H.; Erickson, J.; Mitsuya, H. JE-2147: A dipeptide protease inhibitor (PI) that potently inhibits multi-PI-resistant HIV-1. *Proc. Natl. Acad. Sci. U.S.A.* **1999**, *96*, 8675–8680.

(37) Koh, Y.; Nakata, H.; Maeda, K.; Ogata, H.; Bilcer, G.; Devasamudram, T.; Kincaid, J. F.; Boross, P.; Wang, Y. F.; Ties, Y. F.; Volarath, P.; Gaddis, L.; Harrison, R. W.; Weber, I. T.; Ghosh, A. K.; Mitsuya, H. Novel bis-tetrahydrofuranylurethane-containing nonpeptidic protease inhibitor (PI) UIC-94017 (TMC114) with potent activity against multi-PI-resistant human immunodeficiency virus in vitro. *Antimicrob. Agents Chemother.* **2003**, *47*, 3123–3129.

(38) Markowitz, M.; Conant, M.; Hurley, A.; Schluger, R.; Duran, M.; Peterkin, J.; Chapman, S.; Patick, A.; Hendricks, A.; Yuen, G. J.; Hoskins, W.; Clendeninn, N.; Ho, D. D. *A preliminary evaluation of nelfinavir mesylate, an inhibitor of human immunodeficiency virus (HIV)-1 protease, to treat HIV infection*; University of Chicago Press: Chicago, 1998; pp 1533−1540.

(39) Wlodawer, A.; Erickson, J. W. Structure-Based Inhibitors of HIV-1 Protease. *Annu. Rev. Biochem.* **1993**, *62*, 543–585.

(40) Johnson, V. A.; Brun-Vezinet, F.; Clotet, B.; Conway, B.; Kuritzkes, D. R.; Pillay, D.; Schapiro, J.; Telenti, A.; Richman, D. Update of the drug resistance mutations in HIV-1. *Top. HIV Med. 2005* **2005**, *13*, 51–57.

(41) Baldwin, E. T.; Bhat, T. N.; Liu, B. S.; Pattabiraman, N.; Erickson, J. W. Structural basis of drug-resistance for the V82A mutant of HIV-1 proteinase. *Nat. Struct. Biol.* **1995**, *2*, 244–249.

(42) Maeda, K.; Yoshimura, K.; Shibayama, S.; Habashita, H.; Tada, H.; Sagawa, K.; Miyakawa, T.; Aoki, M.; Fukushima, D.; Mitsuya, H. Novel low molecular weight spirodiketopiperazine derivatives potently inhibit R5 HIV-1 infection through their antagonistic effects on CCR5. *J. Biol. Chem.* **2001**, *276*, 35194–35200.

(43) Kim, E. E.; Baker, C. T.; Dwyer, M. D.; Murcko, M. A.; Rao, B. G.; Tung, R. D.; Navia, M. A. Crystal-Structure of HIV-1 Protease in Complex with VX-478, a Potent and Orally Bioavailable Inhibitor of the Enzyme. *J. Am. Chem. Soc.* **1995**, *117*, 1181–1182.

(44) Wlodawer, A.; Vondrasek, J. Inhibitors of HIV-1 protease: A major success of structure-assisted drug design. *Annu. Rev. Biophys. Biomol. Struct.* **1998**, *27*, 249–284.

(45) Thaisrivongs, S.; Skulnick, H. I.; Turner, S. R.; Strohbach, J. W.; Tommasi, R. A.; Johnson, P. D.; Aristoff, P. A.; Judge, T. M.; Gammill, R. B.; Morris, J. K.; Romines, K. R.; Chrusciel, R. A.; Hinshaw, R. R.; Chong, K. T.; Tarpley, W. G.; Poppe, S. M.; Slade, D. E.; Lynn, J. C.; Horng, M. M.; Tomich, P. K.; Seest, E. P.; Dolak, L. A.; Howe, W. J.; Howard, G. M.; Schwende, F. J.; Toth, L. N.; Padbury, G. E.; Wilson, G. J.; Shiou, L. H.; Zipp, G. L.; Wilkinson, K. F.; Rush, B. D.; Ruwart, M. J.; Koeplinger, K. A.; Zhao, Z. Y.; Cole, S.; Zaya, R. M.; Kakuk, T. J.; Janakiraman, M. N.; Watenpaugh, K. D. Structure-based design of HIV protease inhibitors: Sulfonamide-containing 5,6-dihydro-4-hydroxy-2-pyrones as non-peptidic inhibitors. *J. Med. Chem.* **1996**, *39*, 4349–4353.

(46) Turner, S. R.; Strohbach, J. W.; Tommasi, R. A.; Aristoff, P. A.; Johnson, P. D.; Skulnick, H. I.; Dolak, L. A.; Seest, E. P.; Tomich, P. K.; Bohanan, M. J.; Horng, M. M.; Lynn, J. C.; Chong, K. T.; Hinshaw, R. R.; Watenpaugh, K. D.; Janakiraman, M. N.; Thaisrivongs, S. Tipranavir (PNU-140690): A potent, orally bioavailable nonpeptidic HIV protease inhibitor of the 5,6-dihydro-4-hydroxy-2-pyrone sulfonamide class. *J. Med. Chem.* **1998**, *41*, 3467–3476.

(47) Brown, K. L.; Bren, U.; Stone, M. P.; Guengerich, F. P. Inherent stereospecificity in the reaction of aflatoxin B1 8,9-epoxide with deoxyguanosine and efficiency of DNA catalysis. *Chem. Res. Toxicol.* **2009**, *22*, 913–917.

(48) McGovern, S. L.; Caselli, E.; Grigorieff, N.; Shoichet, B. K. A common mechanism underlying promiscuous inhibitors from virtual and high-throughput screening. *J. Med. Chem.* **2002**, *45*, 1712–1722.
(49) Shoichet, B. K. Screening in a spirit haunted world. *Drug Discovery Today* **2006**, *11*, 607–615.
(50) Ode, H.; Matsuyama, S.; Hata, M.; Hoshino, T.; Kakizawa, J.; Sugiura, W. Mechanism of drug resistance due to N88S in CRF01_AE HIV-1 protease, analyzed by molecular dynamics simulations. *J. Med. Chem.* **2007**, *50*, 1768–1777.
(51) Ode, H.; Matsuyama, S.; Hata, M.; Neya, S.; Kakizawa, J.; Sugiura, W.; Hoshino, T. Computational characterization of structural role of the non-active site mutation M36I of human immunodeficiency virus type 1 protease. *J. Mol. Biol.* **2007**, *370*, 598–607.
(52) Ode, H.; Neya, S.; Hata, M.; Sugiura, W.; Hoshino, T. Computational simulations of HIV-1 proteases-multi-drug resistance due to nonactive site mutation L90M. *J. Am. Chem. Soc.* **2006**, *128*, 7887–7895.

CI900320P

THE JOURNAL OF BIOLOGICAL CHEMISTRY VOL. 284, NO. 51, pp. 35681–35691, December 18, 2009
Printed in the U.S.A.

Mechanism of Inhibition of HIV-1 Reverse Transcriptase by 4′-Ethynyl-2-fluoro-2′-deoxyadenosine Triphosphate, a Translocation-defective Reverse Transcriptase Inhibitor*

Received for publication, June 23, 2009, and in revised form, October 14, 2009 Published, JBC Papers in Press, October 16, 2009, DOI 10.1074/jbc.M109.036616

Eleftherios Michailidis[‡], Bruno Marchand[‡1], Eiichi N. Kodama[§2], Kamlendra Singh[‡], Masao Matsuoka[§], Karen A. Kirby[‡], Emily M. Ryan[‡], Ali M. Sawani[‡], Eva Nagy[¶], Noriyuki Ashida[‖], Hiroaki Mitsuya[‡‡], Michael A. Parniak[¶], and Stefan G. Sarafianos[‡3]**

From the [‡]Christopher Bond Life Sciences Center, Department of Molecular Microbiology and Immunology, University of Missouri, Columbia, Missouri 65211, the [§]Institute for Virus Research, Kyoto University, Kyoto 606-8507, Japan, the [¶]Department of Molecular Genetics and Biochemistry, University of Pittsburgh, Pittsburgh, Pennsylvania 15261, [‖]Yamasa Corporation, Chiba 288-0056, Japan, the [**]Department of Hematology and Infectious Diseases, Kumamoto University, Kumamoto 860-8556, Japan, and the [‡‡]Experimental Retrovirology Section, HIV/AIDS Malignancy Branch, National Institutes of Health, Bethesda, Maryland 20892

Nucleoside reverse transcriptase inhibitors (NRTIs) are employed in first line therapies for the treatment of human immunodeficiency virus (HIV) infection. They generally lack a 3′-hydroxyl group, and thus when incorporated into the nascent DNA they prevent further elongation. In this report we show that 4′-ethynyl-2-fluoro-2′-deoxyadenosine (EFdA), a nucleoside analog that retains a 3′-hydroxyl moiety, inhibited HIV-1 replication in activated peripheral blood mononuclear cells with an EC_{50} of 0.05 nM, a potency several orders of magnitude better than any of the current clinically used NRTIs. This exceptional antiviral activity stems in part from a mechanism of action that is different from approved NRTIs. Reverse transcriptase (RT) can use EFdA-5′-triphosphate (EFdA-TP) as a substrate more efficiently than the natural substrate, dATP. Importantly, despite the presence of a 3′-hydroxyl, the incorporated EFdA monophosphate (EFdA-MP) acted mainly as a *de facto* terminator of further RT-catalyzed DNA synthesis because of the difficulty of RT translocation on the nucleic acid primer possessing 3′-terminal EFdA-MP. EFdA-TP is thus a translocation-defective RT inhibitor (TDRTI). This diminished translocation kept the primer 3′-terminal EFdA-MP ideally located to undergo phosphorolytic excision. However, net phosphorolysis was not substantially increased, because of the apparently facile reincorporation of the newly excised EFdA-TP. Our molecular modeling studies suggest that the 4′-ethynyl fits into a hydrophobic pocket defined by RT residues Ala-114, Tyr-115, Phe-160, and Met-184 and the aliphatic chain of Asp-185. These interactions, which contribute to both enhanced RT utilization of EFdA-TP and difficulty in the translocation of 3′-terminal EFdA-MP primers, underlie the mechanism of action of this potent antiviral nucleoside.

Nucleoside reverse transcriptase inhibitors (NRTIs)[4] are central components of first line regimens for treatment of HIV infections (1–6). Currently, there are eight clinically approved NRTIs: AZT, 3TC, FTC, ABC, ddI, ddC, d4T, and the nucleotide tenofovir (TFV; reviewed in Refs. 7 and 8). A structural hallmark of these NRTIs is the lack of a 3′-OH; it has long been considered that the absence of the 3′-OH is essential for antiviral activity. However, the absence of the 3′-OH in NRTIs also imparts detrimental properties to the inhibitor, including reduced affinity for RT compared with the analogous dNTP substrate, as well as reduced intracellular conversion to the active nucleoside triphosphate (9).

Previously we described a series of 4′-substituted NRTIs (10) that retain the 3′-OH group and have excellent antiviral properties and significantly improved selectivity indices (CC_{50}/EC_{50}) compared with the approved NRTIs. Furthermore, these NRTIs efficiently suppress various NRTI-resistant HIV. The most potent of these 4′-substituted NRTIs are the adenosine analogs that have an ethynyl group at the 4′ position of the ribose ring. Despite their high anti-HIV activity, 4′-substituted compounds are susceptible to degradation by adenosine deaminase (11), a property that limits the plasma and intracellular half-life of the drugs. To overcome the adenosine deaminase sensitivity of these 4′-ethynyl NRTIs, we developed a second generation of analogs substituted at the 2-position of the adenine ring (12). We recently reported that the 2-halogenated, 4′-ethynyl compounds have remarkably improved potency and selectivity indices (CC_{50}/EC_{50}) compared with the nonhalogenated analogs and significantly better ones compared with

* This work was supported, in whole or in part, by National Institutes of Health Grants AI076119, AI074389, AI076119-S1, and AI076119-02S1 (to S. G. S.) and AI079801 (to M. A. P.).

[1] Recipient of the amfAR Mathilde Krim Fellowship.

[2] Present address: Div. of Emerging Infectious Diseases, Tohoku University School of Medicine, Sendai 980-8575, Japan.

[3] To whom correspondence should be addressed: 471d Christopher S. Bond Life Sciences Ctr., 1201 Rollins St., Columbia, MO 65211. Tel.: 573-882-4338; E-mail: sarafianoss@missouri.edu.

[4] The abbreviations used are: NRTI, nucleoside reverse transcriptase inhibitor; TDRTI, translocation-defective RT inhibitor; RT, reverse transcriptase; HIV, human immunodeficiency virus; EFdA, 4′-ethynyl-2-fluoro-2′-deoxyadenosine; MP, monophosphate; TP, triphosphate; AZT, azidothymidine; EdA, 4′-ethynyl-2′-deoxyadenosine; EFddA, 4′-ethynyl-2-fluoro-2′,3′-dideoxyadenosine; EFd4A, 4′-ethynyl-2-fluoro-2′,3′-dihydro-2′,3′-dideoxyadenosine; Ed4T, 4′-ethynyl-2′,3′-dihydro-3′-deoxythymidine; TFV, tenofovir; PBMC, peripheral blood mononuclear cell; T/P, template/primer; $T/P_{EFdA\text{-}MP}$ or $T/P_{ddA\text{-}MP}$, template/primer possessing either EFdA-MP or ddAMP at the 3′-primer terminus (or T/P chain terminated by EFdA or ddA); N-site, nucleotide-binding site; P-site, primer site; PDB, Protein Data Bank; d4T, stavudine.

TABLE 1

DNA and RNA sequences used in this study

The primers were fluorescently labeled at the 5′-end except for the footprinting experiments, in which the template was fluorescently labeled at the 5′-end.

Polymerization experiments	
T_{d100}	5′-TAG TGT GTG CCC GTC TGT TGT GTG ACT CTG GTA ACT AGA GAT CCC TCA GAC CCT TTT AGT CAG TGT GGA AAA TCT CTA GCA GTG GCG CCC GAA CAG GGA C
P_{d18}	5′-Cy3 GTC CCT GTT CGG GCG CCA
T_{d31}	5′-CCA TAG CTA GCA TTG GTG CTC GAA CAG TGA C
T_{r31}	5′-CCA UAG CUA GCA UUG GUG CUC GAA CAG UGA C
P_{d18}	5′-Cy3 GTC ACT GTT CGA GCA CCA
Gel shift experiments	
T_{d43}	5′-AAT CAG TGT AGA CAA TCC CTA GCA TTG GTG CTC GAA CAG TGA C
P_{d18}	5′-Cy3 GTC CCT GTT CGG GCG CCA
Footprinting experiments	
P_{d20}	5′-TTG TCA CTG TTC GAG CAC CA
T_{d43}	5′-Cy3 CCA TAG CTA GCA TTG GTG CTC GAA CAG TGA CAA TCA GTG TAGA

other approved NRTIs. These compounds are resistant to degradation by adenosine deamination (13). The most potent of these compounds is EFdA (Fig. 1*A*), which was recently shown not to inhibit human DNA polymerases α and β or mitochondrial DNA polymerase γ (12). Notably, clinically important drug-resistant HIVs (14, 15) are sensitive or hypersensitive to this compound (13).

Despite its remarkable antiviral potency, the molecular mechanism by which EFdA and related compounds inhibit HIV is unknown. To elucidate this mechanism we carried out biochemical experiments that systematically decipher the effect of EFdA on each of the mechanistic steps of DNA synthesis by HIV RT. On the basis of these experiments we propose that EFdA-5′-triphosphate (EFdA-TP) inhibits RT by first being incorporated at the 3′-primer terminus, and after its incorporation it prevents further addition of nucleotides by blocking the translocation of the primer strand on the viral polymerase. We therefore termed EFdA a "translocation-defective reverse transcriptase inhibitor (TDRTI)." By understanding the molecular details of RT inhibition by a highly potent NRTI, we hope to gain insights into the design of even more efficacious inhibitors that may act via same or similar mechanisms.

EXPERIMENTAL PROCEDURES

Enzymes and Nucleic Acids

The RT genes coding for p66 and p51 subunits of BH10 HIV-1 were cloned in the pETDuet-1 vector (Novagen) using restriction sites NcoI and SacI for the p51 subunit and SacII and AvrII for the p66 subunit. The sequences coding for a hexahistidine tag and the 3C protease recognition sequence were added at the N terminus of the p51 subunit. RT was expressed in BL21 (Invitrogen) and purified by nickel affinity chromatography and MonoQ anion exchange chromatography (16). Oligonucleotides used in this study were synthesized chemically and purchased from Integrated DNA Technologies (Coralville, IA). Sequences of the DNA/RNA substrates are shown in Table 1. Deoxynucleotide triphosphates and dideoxynucleotide triphosphates were purchased from Fermentas (Glen Burnie, MD). EFdA was synthesized by Yamasa Corp. (Chiba, Japan) as described previously (12). Using EFdA as the starting material, the triphosphate form, EFdA-TP, was synthesized by TriLink BioTechnologies (San Diego, CA). Concentrations of nucleotides and EFdA-TP were calculated spectrophotometrically on the basis of absorption at 260 nm and their extinction coefficients. All nucleotides were treated with inorganic pyrophosphatase (Roche Diagnostics) as described previously (17) to remove traces of PP_i contamination that might interfere with the rescue assay.

Cell-based HIV-1 Replication Assays

Peripheral blood mononuclear cells (PBMCs) were isolated from healthy donor buffy coats (purchased from the Central Blood Bank, Pittsburgh, PA) using Ficoll-Hypaque (Histopaque, Sigma-Aldrich) gradient centrifugation as described previously (18). PBMCs were stimulated with 5 μg/ml phytohemagglutinin (Sigma) in RPMI 1640 containing 10% fetal bovine serum for 48 h prior to exposure to drug and virus. After washing, the activated cells were resuspended in RPMI 1640/fetal bovine serum containing interleukin-2 (10 units/ml) and varying concentrations of the NRTIs and then were infected with HIV-1_{NL4-3} at a multiplicity of infection of 0.01. HIV-1 infection was assessed by measuring HIV-1 p24 antigen in cell-free culture supernatants obtained 7 days post-infection using an HIV-1 p24 antigen capture assay kit (SAIC, Frederick, MD).

Primer Extension Assays

Characterization of EFdA-TP as a Chain Terminator—DNA or RNA template was annealed to a 5′-Cy3-labeled DNA primer (3:1 molar ratio). To monitor the primer extension, the DNA/DNA or RNA/DNA hybrid (20 nM) was incubated at 37 °C with HIV-1 RT (20 nM) in a buffer containing 50 mM Tris (pH 7.8) and 50 mM NaCl (RT buffer). Subsequently, varying amounts of EFdA-TP or ddATP were added, and the reactions were initiated by the addition of 6 mM $MgCl_2$ to a final volume of 20 μl. All dNTPs were present at a final concentration of 1 μM. The reactions were terminated after 15 min by adding an equal volume of 100% formamide containing traces of bromphenol blue. The products were resolved on a 15% polyacrylamide 7 M urea gel. In this and subsequent assays, the gels were scanned with a phosphorimaging device (FLA 5000, FujiFilm). The bands for fully extended product were quantified using Multi Gauge software (FujiFilm), and the results were plotted as percent full extension using GraphPad Prism 4 to determine the IC_{50} for EFdA-TP and other nucleotide analogs.

Steady State Kinetics—Steady state kinetic parameters, K_m and k_{cat}, for incorporation of EFdA-MP or dAMP were determined using single nucleotide incorporation in gel-based assays under saturating substrate conditions. The reactions were car-

ried out in RT buffer with 6 mM $MgCl_2$, 100 nM T_{d31}/P_{d18} or T_{r31}/P_{d18}, and 2.5 nM RT in a final volume of 20 μl and stopped at the indicated reaction times. The products were resolved and quantified as described above. K_m and k_{cat} were determined graphically using the Michaelis-Menten equation.

Incorporation of dNTP to the Template/Primer (T/P) Possessing Either EFdA-MP (T/P$_{EFdA-MP}$) or ddAMP (T/P$_{ddAMP}$) at the 3′-Primer Terminus—$T/P_{EFdA-MP}$ and T/P_{ddAMP} were prepared by incubating 500 nM T_{d31}/P_{d18} with 1 μM HIV-1 RT in RT buffer and 6 mM $MgCl_2$. EFdA-TP (1 μM) or ddATP (5 μM) was added into the reaction and the mixture was incubated at 37 °C for 1 h. After incorporation of the nucleotide analogs, the T/P_{analog} was purified using the QIAquick nucleotide removal kit (Qiagen, Valencia, CA). Under these conditions, the extension of T/P to $T/P_{EFdA-MP}$ or T/P_{ddAMP} was complete. Purified $T/P_{EFdA-MP}$ (5 nM) was incubated with 20 nM HIV-1 RT in RT buffer and 6 mM $MgCl_2$. The first incoming nucleotide was added at different concentrations (0–100 μM) in the presence of the other dNTPs (1 μM). The reactions were incubated at 37 °C for 15 or 60 min.

Gel Mobility Shift Assays

Formation of RT·DNA Binary Complex—$T/P_{EFdA-MP}$ and T/P_{ddAMP} were prepared using T_{d43}/P_{d18} as described above. Purified $T/P_{EFdA-MP}$ or T/P_{ddAMP} (20 nM) was incubated at room temperature for 10 min with different concentrations of HIV-1 RT in RT buffer and 6 mM $MgCl_2$. RT was used at different concentrations to obtain RT/DNA ratios that ranged from 0.25 to 7.5. Four μl of 20% sucrose was added to each mixture in a final volume of 20 μl. The complexes were subsequently resolved on a native 6% polyacrylamide Tris borate gel and visualized as described above.

Formation of RT·DNA$_{EFdA-MP}$·dTTP Ternary Complex—Purified $T/P_{EFdA-MP}$ or T/P_{ddAMP} (9 nM) was incubated at room temperature for 10 min with 100 nM HIV-1 RT, varying amounts of the next nucleotide (1–5000 μM) in RT buffer, and 6 mM $MgCl_2$. Prior to the addition of sucrose, 150 ng/μl heparin was added, and finally the products were resolved on native 6% polyacrylamide Tris borate gels and visualized as described above.

Site-specific Fe^{2+} Footprinting Assay

Site-specific Fe^{2+} footprints were monitored on 5′-Cy3-labeled DNA templates. T_{d43}/P_{d20} (100 nM) was incubated with HIV-1 RT (600 nM) in a buffer containing 120 mM sodium cacodylate (pH 7), 20 mM NaCl, 6 mM $MgCl_2$, and EFdA-TP (1 μM) to allow quantitative chain termination. Prior to treatment with Fe^{2+}, complexes were preincubated for 7 min with increasing concentrations of the next nucleotide as indicated in Fig. 5*A*. The complexes were treated with ammonium iron sulfate (1 mM) as described previously (19). This reaction relies on autoxidation of Fe^{2+} (20) to create a local concentration of the hydroxyl radical, which cleaves the DNA at the nucleotide closest to the Fe^{2+} specifically bound to the RNase H active site.

PP_i- and ATP-dependent Excision and Rescue of $T/P_{EFdA-MP}$ and T/P_{ddAMP}

PP_i-dependent Excision of $T/P_{EFdA-MP}$ and T/P_{ddAMP}—Purified $T/P_{EFdA-MP}$ and T/P_{ddAMP} (20 nM) were incubated at 37 °C with HIV-1 RT (60 nM) in the presence of 150 μM PP_i in RT buffer and 6 mM $MgCl_2$. Aliquots of the reaction were stopped at different times (0–30 min) and analyzed as described above.

PP_i-dependent Rescue of $T/P_{EFdA-MP}$ and T/P_{ddAMP}—Purified $T/P_{EFdA-MP}$ and T/P_{ddAMP} (20 nM) were incubated with HIV-1 RT (60 nM) at various concentrations of PP_i (0–150 μM) in RT buffer and 6 mM $MgCl_2$. The assay was performed in the presence of a large excess of competing dATP (100 μM), which prevented reincorporation of EFdA-MP, 0.5 μM dTTP, and 10 μM ddGTP. After an incubation of 10 min at 37 °C, the reactions were stopped and analyzed as described above.

ATP-dependent Rescue of $T/P_{EFdA-MP}$ and T/P_{ddAMP}—Purified $T/P_{EFdA-MP}$ and T/P_{ddAMP} (20 nM) were incubated with HIV-1 RT (60 nM) in the presence of 3.5 mM ATP, 100 μM dATP, 0.5 μM dTTP, and 10 μM ddGTP in RT buffer and 10 mM $MgCl_2$. Aliquots of the reaction were stopped at different time points (0–90 min) and analyzed as described above.

Molecular Modeling

Molecular models of two reaction intermediates that involve EFdA were built as follows. 1) A model of the ternary complex of HIV-1 RT·DNA·EFdA-TP (Fig. 7*A*) was built starting with the coordinates of the crystal structure of the HIV-1 RT·DNA·TFV-DP complex. The triphosphate of EFdA-TP was built using as a guide the corresponding atoms of TFV-DP in structure with PDB code 1T05 and of dTTP in PDB code 1RTD. The coordinates of the 4′-ethynyl sugar ring were from our NMR structure of EFdA[5] showing that EFdA is in a North conformation similar to the sugar puckering observed in the crystal structure of 4′-ethynyl-2′-deoxycytidine (21). The structure of the EFdA-TP was assembled from its components using the sketch module of Sybyl 7.0 (Tripos Associates, St. Louis, MO), and minimized by the semiempirical quantum chemical method PM3 (22). The PM3 charges and the docking module of Sybyl 7.0 were used to dock the EFdA-TP at the RT dNTP-binding site (after removing the TFV-DP from 1T05) to generate the ternary complex HIV-1 RT·T/P·EFdA-TP. The final complex structure was minimized for 100 cycles using the AMBER force field with Coleman united charges on the protein and DNA molecules. 2) The model of the RT·$T/P_{EFdA-MP}$ binary complex with primer 3′-terminal EFdA-MP at the pre-translocation nucleotide-binding site (N-site) (or dNTP-binding site) (Fig. 7*B*) was built using as a starting model our crystal structure of the pre-translocation complex RT·T/P_{AZT-MP} (PDB code 1N6Q). The structures of AZTMP and the base-pairing dA were replaced by EFdA-MP (built as in EFdA-TP above) and a dT, respectively, using the sketch module of Sybyl 7.0, and energy-minimized using the AMBER force field with Coleman united charges on the protein and DNA molecules.

[5] K. A. Kirby, K. Singh, E. Michailidis, B. Marchand, E. N. Kodama, E. Nagy, N. Ashida, H. Mitsuya, M. A. Parniak, and S. G. Sarafianos, unpublished data.

RESULTS

EFdA-TP Is a Highly Potent Inhibitor of HIV-1 RT—EFdA inhibits HIV-1 replication in phytohemagglutinin-activated PBMCs with an EC_{50} of 50 pM (Table 2), consistent with previously published data obtained using T-cell lines (12, 13), and data published after completion of this work (23). The antiviral potency of EFdA is at least 4 orders of magnitude greater than the clinically used adenine nucleotide analog tenofovir and over 400-fold greater than that of AZT when assessed under the same conditions (Table 2). EFdA thus appears to be the most potent nucleoside inhibitor described to date of HIV-1 replication in primary cells. It is also interesting to note that EFdA is substantially more potent than analogs lacking a 3′-OH function (EFddA and EFd4A; Table 2). No cytotoxicity was noted at 10 μM EFdA (data not shown), the highest concentration tested, suggesting an *in vitro* selectivity index of over 200,000. To better understand the molecular basis for the exceptional antiviral potency of EFdA, we carried out a series of detailed *in vitro* evaluations of the impact of the active antiviral form of EFdA, namely EFdA-TP, on DNA synthesis catalyzed by purified HIV-1 RT.

TABLE 2
Inhibition of HIV-1 replication in phytohemagglutinin-activated PBMCs by EFdA, EFdA analogs, and other NRTIs

Compound	EC_{50}[a]
	nM
EFdA	0.05 ± 0.02
EdA	11 ± 7
EFddA	570 ± 92
EFd4A	14 ± 11
Zidovudine (or AZT)	22 ± 7
Tenofovir	3300 ± 1240

[a] Values are means ± S.D. of triplicate determinations and were determined by assessment of reduction in HIV-1 p24 antigen production in infected cells as described under "Experimental Procedures."

We first compared the effect of EFdA-TP with other NRTI-TPs (ddATP, TFV-DP, AZTTP, and ddCTP) on RT-catalyzed DNA synthesis in *in vitro* primer extension assays using a nucleic acid T/P comprising a 100-nucleotide DNA template annealed to a Cy3–5′-labeled 18-nucleotide DNA primer (Table 1). As shown in Fig. 1*B*, EFdA-TP suppressed full-length DNA synthesis by RT in a dose-dependent manner. EFdA-TP was between ~1 and 2 orders of magnitude more effective at inhibiting RT-catalyzed DNA synthesis than any of the NRTIs evaluated. The IC_{50} for suppression of full primer extension by EFdA-TP was 14 nM using the longer T_{d100}/P_{d18} (Fig. 1, *C* and *D*). To confirm the high efficiency at which RT uses EFdA, we performed single nucleotide incorporation assays under steady state conditions (using T_{d31}/P_{d18} or T_{r31}/P_{d18} as a T/P, Table 1). Our results show that under these conditions the incorporation efficiency (k_{cat}/K_m) of EFdA-TP by RT is twice that for the natural dATP substrate and four times that for ddATP, primarily because of changes in the K_m of RT to these substrates (Table 3). Moreover, we found that the increase in incorporation efficiency of EFdA-TP could be even higher at different nucleic acid sub-

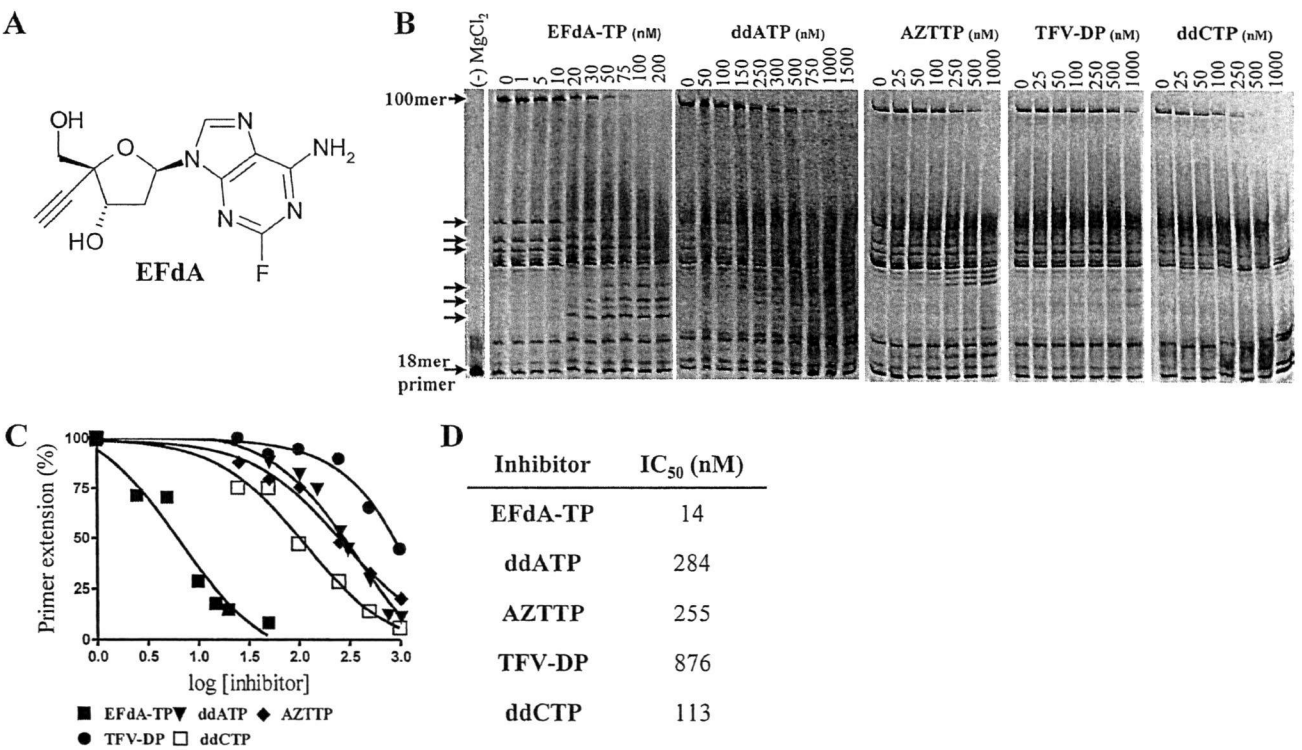

FIGURE 1. **HIV RT inhibition by EFdA-TP and other NRTIs.** *A*, structure of EFdA. *B*, primer extension by HIV-1 RT was observed in the presence of fixed concentrations of 4 dNTPs, T_{d100}/P_{d18}, and $MgCl_2$ and increasing concentrations of EFdA-TP, ddATP, AZTTP, TFV-DP, or ddCTP. The reactions were carried out for 15 min. The *arrows* denote stops of the elongating DNA chain where adenosine analogs (EFdA-TP, ddATP, or TFV-DP) were expected to be incorporated. The *first lane* is a negative control, where no $MgCl_2$ was added; it shows the length of the 18-mer primer. *C*, the 100-mer products synthesized by HIV-1 RT were quantified and plotted against increasing concentrations of various inhibitors. The data points were fitted by GraphPad Prism 4. *D*, IC_{50} values of the nucleotide analogs were determined by quantifying the percent of full extension and fitting the data points to GraphPad Prism 4 using one-site competition nonlinear regression.

TABLE 3

Steady state kinetic parameters (K_m and k_{cat}) for EFdA-MP and dAMP incorporation by HIV-1 RT

Values are means ± S.D. of triplicate determinations and were determined from Michaelis-Menten equation using GraphPad Prism 4. ND, not determined.

dNTP	T/P (DNA/DNA)				T/P (RNA/DNA)			
	K_m	k_{cat}	k_{cat}/K_m	Selectivity[a]	K_m	k_{cat}	k_{cat}/K_m	Selectivity[a]
	nM	min^{-1}	$min^{-1}\cdot nM^{-1}$		nM	min^{-1}	$min^{-1}\cdot nM^{-1}$	
dATP	73.11 ± 11	19.9 ± 0.7	0.272	1	21.3 ± 8	3.1 ± 0.2	0.145	1
EFdA-TP	39.2 ± 3	21.1 ± 0.4	0.538	2	24.1 ± 5	2.3 ± 0.1	0.095	0.7
ddATP	97.0 ± 9	15.4 ± 0.3	0.159	0.6	ND	ND	ND	ND

[a] Selectivity is the ratio of the incorporation efficiency (k_{cat}/K_m) of EFdA-MP or ddAMP over that of dAMP ($[k_{cat}/K_m]_{EFdA\text{-}MP}/[k_{cat}/K_m]_{dAMP}$ or $[k_{cat}/K_m]_{ddAMP}/[k_{cat}/K_m]_{dAMP}$).

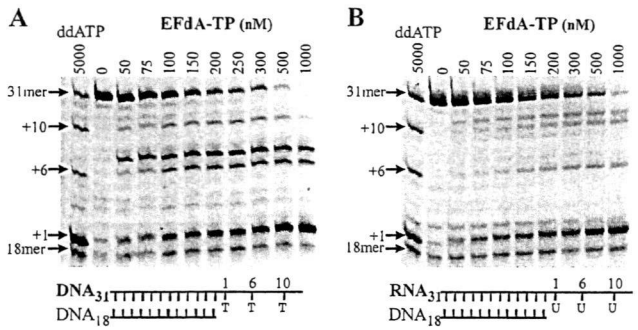

FIGURE 2. **Inhibition of DNA- and RNA-dependent DNA synthesis by EFdA-TP.** *A*, T_{d31}/P_{d18} was incubated with HIV-1 RT for 15 min in the presence of 1 μM dNTPs and $MgCl_2$ and increasing concentrations of EFdA-TP (0–1000 nM). The *first lane* (dd*ATP*) shows the inhibition of primer extension by ddATP to identify points of adenosine analog (ddATP or EFdA-TP) incorporation (*arrows*: +1, +6, and +10). *B*, the primer extension under the same conditions with an RNA/DNA substrate containing an RNA template annealed to a DNA primer (T_{r31}/P_{d18}).

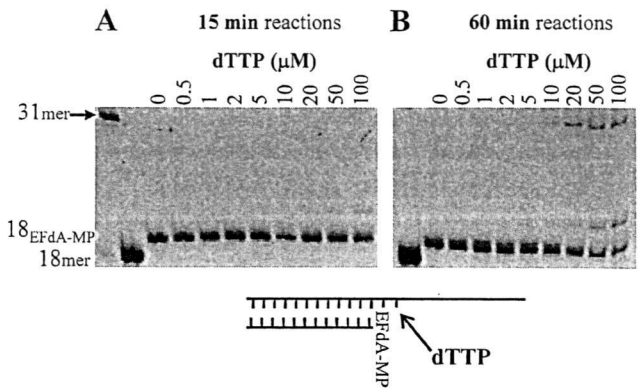

FIGURE 3. **Incorporation of dNTP on EFdA-terminated template/primer ($T/P_{EFdA\text{-}MP}$).** EFdA-TP was first incorporated at T_{d31}/P_{d18} by HIV-1 RT and purified as described under "Experimental Procedures." The incorporation of the next incoming nucleotide on $T/P_{EFdA\text{-}MP}$ was examined in the presence of HIV-1 RT and $MgCl_2$ and increasing concentrations of dTTP. All other dNTPs were at a concentration of 1 μM. The reactions were stopped after 15 min (*A*) and 60 min (*B*).

strate sequences, more than 10 times higher than dATP (data not shown).

The EFdA-TP-mediated reduction in full-length DNA synthesis was accompanied by the concomitant appearance of products corresponding to the primer extension only at the length expected for the incorporation of adenosine nucleotides (indicated by *arrows* in Fig. 1*B*). Neither ddATP nor TFV-DP provided significant accumulation of this small DNA product.

EFdA-TP Inhibits DNA Synthesis Mainly at the Point of Incorporation—The stopping patterns of DNA synthesis were different in the presence of EFdA-TP compared with other dATP analogs such as ddATP and TFV-DP (marked by *arrows* in Fig. 1*B*). Hence, we used a shorter template (T_{d31}/P_{d18} (Table 1)), which allowed unambiguous identification of the stopping sites. As expected, the inhibitory potential of EFdA (and other NRTIs) appears lower in these shorter T/P (IC_{50} for suppression of full primer extension was 104 nM) in which there are fewer opportunities for incorporation (24). This substrate allows incorporation of dA, ddA, or EFdA at positions 1, 6, and 10 (Fig. 2). The results show that EFdA-TP causes major pauses at all possible points of incorporation ((Fig. 2*A*, positions 1, 6, and 10), suggesting that EFdA-TP inhibits RT mainly as an obligate chain terminator. Notably, there was a distinct difference at position +6 of T_{d31}/P_{d18}, where we observed a strong stop not only at the point of incorporation but also at the position following (Fig. 2*A*, positions 6 and 7, respectively). These results suggest that in some cases EFdA-MP may also allow incorporation of an additional nucleotide depending upon the template sequence.

EFdA-TP inhibits both RNA- and DNA-dependent RT-catalyzed full-length DNA polymerization to comparable extents (Fig. 2). The selectivity for incorporation of EFdA-MP over dAMP ($(k_{cat}/K_m)_{EFdA\text{-}TP}/(k_{cat}/K_m)_{dATP}$) was slightly increased when we used DNA/DNA *versus* RNA/DNA template/primers (Table 3, 2 *versus* 0.7). Notably, the overall pausing pattern due to inhibition by EFdA-TP differs depending on whether the template is RNA or DNA. Inhibition differences based on type and sequence of template are currently under investigation.

Extension of EFdA-terminated T/P ($T/P_{EFdA\text{-}MP}$)—The data in Figs. 1 and 2 suggest that EFdA-TP can act as a terminator of RT-catalyzed DNA synthesis in a manner similar to that of other NRTI-TPs. We therefore examined the efficiency of nucleotide additions to primers that were synthesized to already possess a 3′-terminal EFdA-MP. Fig. 3 shows that the primer extension from EFdA-MP is very limited and is evident only at very high and nonphysiological concentrations (>50 μM) of the next nucleotide and with extended reaction times (Fig. 3*B*, 60-min incubation). It therefore appears that EFdA acts as a *de facto* chain terminator, despite the presence of a 3′-OH function.

RT Binds T/P_{ddAMP} and $T/P_{EFdA\text{-}MP}$ at Similar Efficiencies—A possible reason for the inability of RT to efficiently extend the EFdA-MP-terminated primer is that it binds $T/P_{EFdA\text{-}MP}$ with less affinity than it does a T/P lacking a 3′-terminal EFdA-MP nucleotide. We therefore used gel mobility shift assays to compare the stabilities of the binary complexes of RT with T/P possessing either EFdA-MP ($T/P_{EFdA\text{-}MP}$) or ddAMP

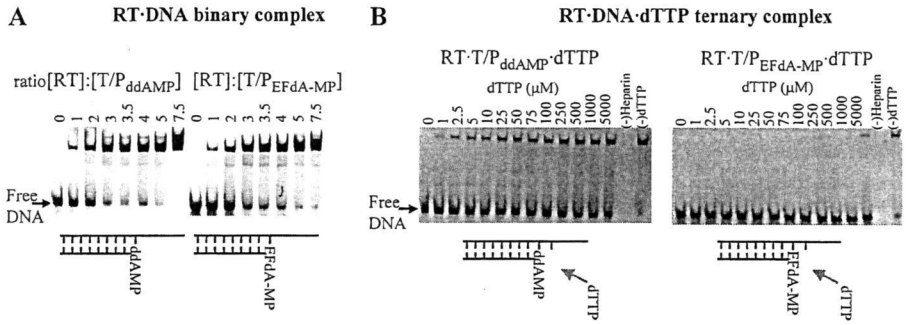

FIGURE 4. **Effect of ddA or EFdA on formation of binary and ternary complexes.** *A*, formation of a binary complex between RT and T/P$_{ddAMP}$ or T/P$_{EFdA-MP}$. Purified T/P$_{ddAMP}$ or T/P$_{EFdA-MP}$ (20 nM) was incubated with HIV-1 RT at the indicated molar ratios and resolved by nondenaturing gel electrophoresis. *B*, formation of a ternary complex between RT and T/P$_{ddAMP}$ or T/P$_{EFdA-MP}$ and incoming dTTP. The stability of the ternary complexes was analyzed by incubating 100 nM RT and 9 nM T/P$_{ddAMP}$ or T/P$_{EFdA-MP}$ in the presence of increasing dTTP concentrations and heparin, which acted as an enzyme trap. In the absence of dTTP, the T/P·RT binary complex is unstable (*lane 0*), as RT dissociates from the T/P and is trapped by heparin.

(T/P$_{ddAMP}$) at the 3′-primer terminus (T/P chain terminated by EFdA-MP or ddAMP). As shown in Fig. 4*A*, RT binds T/P$_{EFdA-MP}$ with an apparent affinity comparable with that of the normal T/P (K_d for RT·T/P$_{EFdA-MP}$ = 51 nM; K_d for RT·T/P$_{ddA-MP}$ = 42 nM). This observation suggests that RT is inhibited at a downstream step in the polymerization reaction.

RT Is Unable to Form a Stable Ternary Complex with T/P$_{EFdA-MP}$ and dNTP—The next step in the DNA polymerization mechanism is the binding of the next complementary dNTP to RT·DNA, thus forming the ternary complex that precedes catalysis. To determine whether EFdA exerts its inhibitory effect by interfering with the formation of a stable ternary complex with the incoming dNTP, we used a gel-based nondenaturing electrophoresis assay (25) that detects the ternary complex formed by RT·T/P and the next complementary dNTP (in this case, dTTP). In this assay, the stability of the ternary complex is assessed by the persistence of the RT·DNA·dNTP complex upon addition of a competing heparin trap (25). As seen in Fig. 4*B* (*left panel*), the ternary complex formed by RT with T/P$_{ddAMP}$ and dTTP is quite stable. In contrast, no significant amount of ternary complex was noted in assays using T/P$_{EFdA-MP}$ even at very high dTTP concentrations (Fig. 4*B*, *right panel*).

Incorporation of EFdA-TP into DNA (T/P$_{EFdA-MP}$) Decreases Translocation of RT—The inability of RT to form a stable ternary complex with T/P$_{EFdA-MP}$ and the next complementary dNTP could arise from several factors including (i) the inability of the 3′-terminal EFdA-MP primer to efficiently translocate from the N-site (which is also the pre-translocation site) to the post-translocation primer site (P-site), thereby preventing the next incoming nucleotide from binding; and (ii) the fact that T/P$_{EFdA-MP}$ *can* translocate, but the presence of unnatural substituents in the primer 3′-terminal EFdA-MP (4′-ethynyl and 2-fluoro) may alter geometric and electronic parameters at the primer end, thus preventing efficient incorporation of the next incoming dNTP such that catalysis cannot occur. These two different possibilities place the nucleic acid at different positions/registers with respect to a site-specific landmark in RT, the metal-binding ribonuclease H (RNase H) active site, as shown in the schematic of Fig. 5*B*. We therefore used a site-specific Fe^{2+} footprinting assay (19) to determine whether the primer 3′-terminal EFdA-MP of the RT·T/P$_{EFdA-MP}$ complex resides primarily in the pre- (N-site) or post-translocation (P-site) state in the absence and the presence of varying levels of the incoming complementary dNTP, which serves to "force" the 3′-primer terminus from the pre-translocation (N-site) to the post-translocation site (P-site). As shown on Fig. 5*A* (*left panel*), in the absence of dTTP (*first lane*), primers with a 3′-terminal ddAMP are located in both the pre- and post-translocation sites in approximately equal amounts, and the addition of the next complementary nucleotide (dTTP) forces the primer 3′-end almost entirely into the post-translocation site. In contrast, in the absence of dTTP, primers with a 3′-terminal EFdA-MP are located exclusively in the pre-translocation site (Fig. 5*A*, *right panel, first lane*). The next complementary nucleotide (dTTP) is unable to shift the position of the 3′-EFdA-MP except at very high (nonphysiological) concentrations.

Because it is physically impossible for the incoming dNTP to bind at the N-site (dNTP-binding site) when it is occupied by the 3′-primer terminus of the non-translocated T/P$_{EFdA-MP}$, the present data demonstrate that the apparent termination of RT-catalyzed DNA synthesis upon incorporation of EFdA-MP arises from the inability of the 3′-EFdA-MP-terminated primer/template (T/P$_{EFdA-MP}$) to efficiently translocate to the P-site and allow incorporation of the next dNTP. Moreover, the latter is unable to force translocation of the 3′-EFdA-MP-terminated primer strand. The inability of the 3′-EFdA-MP-terminated primer to translocate to allow binding of the next complementary dNTP effectively prevents continued elongation of the nascent viral DNA, despite the presence of the 3′-OH on EFdA. Therefore, we propose that EFdA acts as a *translocation-defective reverse transcriptase inhibitor.*

Phosphorolytic Excision of EFdA-MP—Two major mechanisms account for HIV resistance to NRTIs (26). One is based on NRTI discrimination, where the mutant RT preferentially incorporates the natural dNTP rather than the NRTI-TP. The other major resistance mechanism involves ATP-mediated phosphorolytic excision of the incorporated chain-terminating NRTI from the 3′-end of the primer (27, 28). We and others have previously shown that for excision to occur, the 3′-end of the primer must be positioned at the pre-translocation or N-site of RT (19, 29, 30). As we have already shown, the 3′-EFdA-MP-terminated primer strand binds predominantly in a pre-translocation mode. This suggests that EFdA-terminated primers might be especially susceptible to RT-catalyzed phosphorolytic removal of the terminating EFdA-MP. To assess this possibility we carried out primer unblocking experiments using nucleic acid substrates having at the 3′-primer terminus either EFdA-MP or ddAMP (T/P$_{EFdA-MP}$ or T/P$_{ddAMP}$, respectively). The quantitation of results in Fig. 6*A*

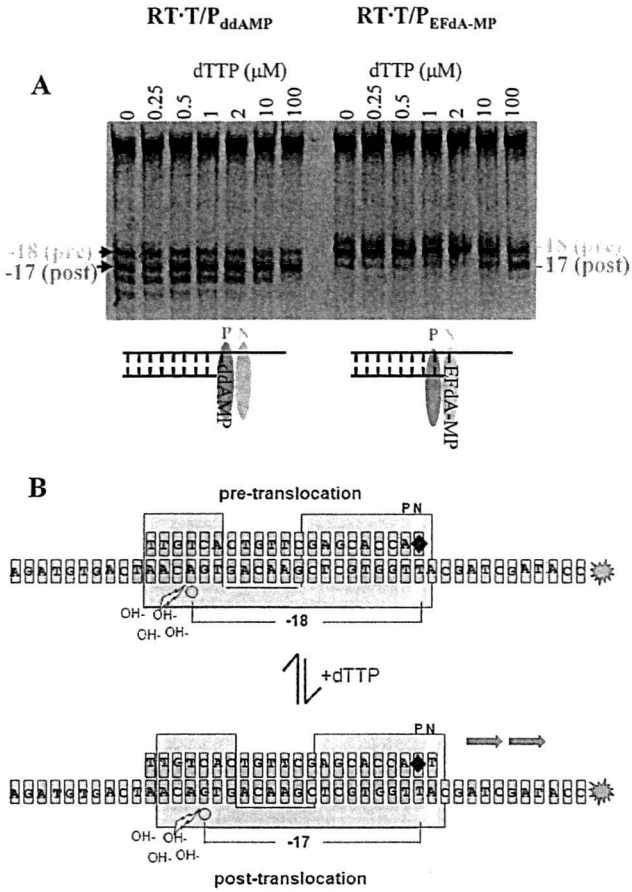

FIGURE 5. **Determination of the translocation state of RT bound to T/P$_{ddAMP}$ and T/P$_{EFdA-MP}$ template/primers.** *A*, the translocation state of RT after EFdA-MP incorporation was determined using site-specific Fe^{2+} footprinting. T/P$_{ddAMP}$ or T/P$_{EFdA-MP}$ (100 nM) with 5′-Cy3 label on the DNA template (see Fig. 5*B*) was incubated with HIV-1 RT (600 nM) and various concentrations of the next incoming nucleotide (dTTP) (as indicated). The complexes were treated for 5 min with ammonium iron sulfate (1 mM) and resolved on a polyacrylamide 7 M urea gel. An excision at position −18 indicates a pre-translocation complex, whereas the excision at position −17 represents a post-translocation complex. The scheme below the gel images indicates that in the absence of incoming dNTP, T/P$_{ddAMP}$ is bound mostly in a post-translocation state, whereas T/P$_{EFdA-MP}$ is bound in a pre-translocation state, with EFdA-MP positioned at the N-site. *B*, schematic of the excision assay. Depending on whether the 3′-primer terminus is positioned at the pre-translocation (N-site) or post-translocation (P-site) site, cleavage is observed on the 5′-labeled template strand at positions −18 or −17, respectively. The addition of varying levels of the incoming complementary dNTP serves to force the 3′-primer terminus from the N-site to the P-site.

shows that the rate of hydrolysis of ddAMP- and EFdA-MP-terminated primers was 0.5 and 1.6 min^{-1}, respectively. We also considered whether the EFdA-TP formed upon pyrophosphorolytic removal of the 3′-terminal EFdA-MP was promptly reincorporated. We tested this possibility using so-called phosphorolysis "rescue" assays, where in addition to the PP_i that would react with the EFdA-MP from the 3′-primer terminus to produce EFdA-TP, we also included a high concentration of dATP that would compete with and prevent reincorporation of EFdA-TP. In the case of high excision activity, we expected to see higher bands corresponding to rescued and extended primers. Indeed, substantially more primer extension was noted in PP_i- or ATP-mediated rescue assays using 3′-terminal EFdA-MP primers (Fig. 6, *C* and *D*, *right panels*) than in assays using primers with 3′-terminal ddAMP (Fig. 6, *C* and *D*, *left panels*). The rate for the ATP-dependent rescue of EFdA-MP-terminated primer was 0.063 min^{-1}. The corresponding rate for the ATP-dependent rescue of the ddAMP-terminated primer could not be calculated because the reaction was very slow. Collectively, these data suggest that 3′-terminal EFdA-MP is phosphorolytically excised more efficiently than ddAMP, consistent with its preferential positioning at the phosphorolysis-susceptible pre-translocation N-site.

Molecular Basis of RT Inhibition by TDRTIs—To understand the molecular basis of RT inhibition by EFdA-TP, we built molecular models of complexes that represent the following intermediates of the DNA polymerization reaction: 1) a pre-catalytic RT·DNA·EFdA-TP ternary complex and 2) a complex that corresponds to the product of EFdA-MP incorporation *prior* to translocation. Previously we had solved crystal structures representing both types of these intermediates for other NRTIs (29, 31), and the model building was guided by the structural characteristics of these complexes. Moreover, we built the EFdA sugar ring in both models in a 3′-endo (North) conformation based on our unpublished NMR experimental data, which clearly show that the equilibrium of the geometries of the EFdA sugar ring overwhelmingly favors the 3′-endo conformation (North). The RT·DNA·EFdA-TP ternary complex model was built using as a starting structure the coordinates of our RT·DNA·TFV-DP crystal structure (PDB code 1T05), not only because it is the highest resolution structure of an RT ternary complex but also because it is the only structure of RT in complex with an analog of deoxyadenosine triphosphate (31). The model of the RT·DNA·EFdA-TP complex represents the step of EFdA-TP binding to the preformed RT·DNA complex (Fig. 7*A*). It had no significant differences from the crystal structures of the ternary complexes of RT with DNA and TFV-DP (PDB code 1T05) or dTTP (PDB code 1RTD). It shows that the 4′-ethynyl of EFdA-TP is favorably positioned in a hydrophobic pocket formed by Ala-114, Tyr-115, Phe-160, and Met-184 and the aliphatic portion of Asp-185. These interactions are similar to those that have been proposed for binding of 4′-Ed4T, a related NRTI thymidine analog that also has a 4′-substitution but no 3′-OH group (32). These interactions are also consistent with the observed high efficiency of EFdA-MP incorporation by RT (Fig. 1*D*). Similar interactions stabilize the RT·DNA$_{EFdA-MP}$ pre-translocation binary complex, which has the primer 3′-terminal EFdA-MP positioned at the N-site (Fig. 7*B*, pre-translocation complex). These favorable interactions are also consistent with the enhanced binding of T/P$_{EFdA-MP}$ in a pre-translocated mode (Fig. 5).

DISCUSSION

The single most distinguishing feature of NRTIs used in HIV therapy is the absence of a 3′-OH. This property results in termination of further viral DNA synthesis upon incorporation of the inhibitor into the nascent viral DNA. We have shown (10, 13) that certain nucleoside analogs that retain the 3′-OH group can exert potent antiviral activity. One of these, EFdA, inhibits HIV-1 replication in PBMCs with a potency that is several orders of magnitude greater than that of any of the current

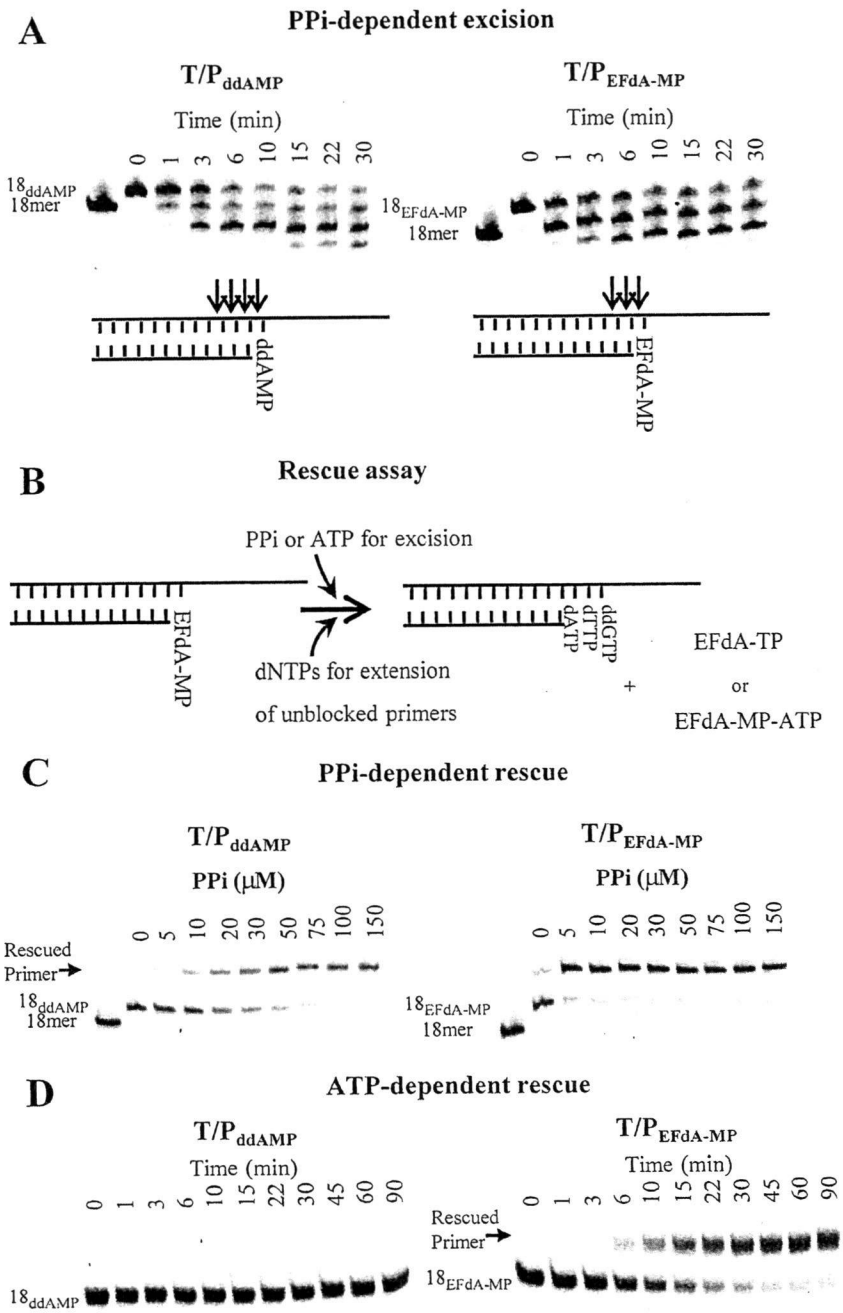

FIGURE 6. **PP_i and ATP-dependent unblocking of ddAMP and EFdA-MP terminated primers.** *A*, PP_i-dependent unblocking of T/P_{ddAMP} and $T/P_{EFdA\text{-}MP}$. Purified T/P_{ddAMP} or $T/P_{EFdA\text{-}MP}$ was incubated with HIV-1 RT in the presence of 6 mM $MgCl_2$ and 150 μM PP_i at 37 °C. Aliquots were removed and reactions stopped at the indicated time points (0–30 min). Cleavage sites are indicated with *arrows* in the schemes below the gels. *B*, schematic representation of PP_i- and ATP-dependent rescue assay. The excision products of PP_i- and ATP-dependent excision of EFdA-MP are EFdA-TP and the EFdA-MP-ATP dinucleoside tetraphosphate, respectively. *C*, PP_i-dependent rescue of T/P_{ddAMP} and $T/P_{EFdA\text{-}MP}$. Purified $T/P_{EFdA\text{-}MP}$ or T/P_{ddAMP} was incubated with HIV-1 RT in the presence of various amounts of PP_i (0–150 μM), dATP (100 μM), dTTP (0.5 μM), or ddGTP (10 μM) and 10 mM $MgCl_2$ at 37 °C. Aliquots of the reaction were stopped after 10 min. *D*, ATP-dependent rescue of T/P_{ddAMP} or $T/P_{EFdA\text{-}MP}$. Purified $T/P_{EFdA\text{-}MP}$ or T/P_{ddAMP} was incubated with HIV-1 RT in the presence of ATP (3.5 mM), dATP (100 μM), dTTP (0.5 μM), or ddGTP (10 μM) and 10 mM $MgCl_2$ at 37 °C. Aliquots of the reaction were stopped at the indicated time points (0–90 min).

clinically used NRTIs (Table 2 and Ref. 23), consistent with the inhibitory data obtained in transformed T-cell lines (13). The molecular basis for this exceptional antiviral activity of EFdA has to date been unclear. The detailed *in vitro* biochemical studies presented in this article show that EFdA inhibits HIV-1 reverse transcriptase mainly by blocking translocation after incorporation at the 3′-primer end and functioning as a TDRTI. The specificity of inhibition can vary depending on the type and sequence of the template (Fig. 2). Our studies also suggest that both the 3′-OH and the 4′-ethynyl groups of EFdA play important roles in the high antiviral potency exerted by this nucleoside analog.

The 4′-ethynyl group is essential for the mechanism of EFdA inhibition of RT-catalyzed DNA synthesis. The present work shows that EFdA-TP acts mainly as a potent terminator of RT-catalyzed DNA synthesis, despite having a 3′-OH group. It is possible that the presence of a 4′-ethynyl substitution on the ribose ring somehow affects the geometry and reactivity of its 3′-OH. However, in the presence of physiological concentrations of dNTPs (<50 μM) the chain terminating activity of EFdA appears to arise mainly from the difficulty of RT to translocate the 3′-EFdA-MP-terminated primer ($T/P_{EFdA\text{-}MP}$) following incorporation of the inhibitor. Under these circumstances the dNTP-binding site is not accessible, and incorporation of the next complementary nucleotide is prevented (Fig. 7*C*). Hence, EFdA appears to act as a translocation-defective RT inhibitor. The 4′-ethynyl moiety appears to be the critical factor in the difficulty presented by translocation of DNA primers with a 3′-terminal EFdA-MP residue. Our molecular model of the RT·DNA·EFdA-TP ternary complex suggests that the 4′-ethynyl moiety fits nicely into a hydrophobic pocket in the RT active site defined by residues Ala-114, Tyr-115, Phe-160, and Met-184 and the aliphatic portion of Asp-185 (Fig. 7*A*), similar to the proposed interactions of 4′-Ed4T at the same site (32). Once EFdA-MP has been added to the primer end to form the pre-translocation (or N-site) reaction product, these same RT residues serve to stabilize the terminal EFdA-MP in

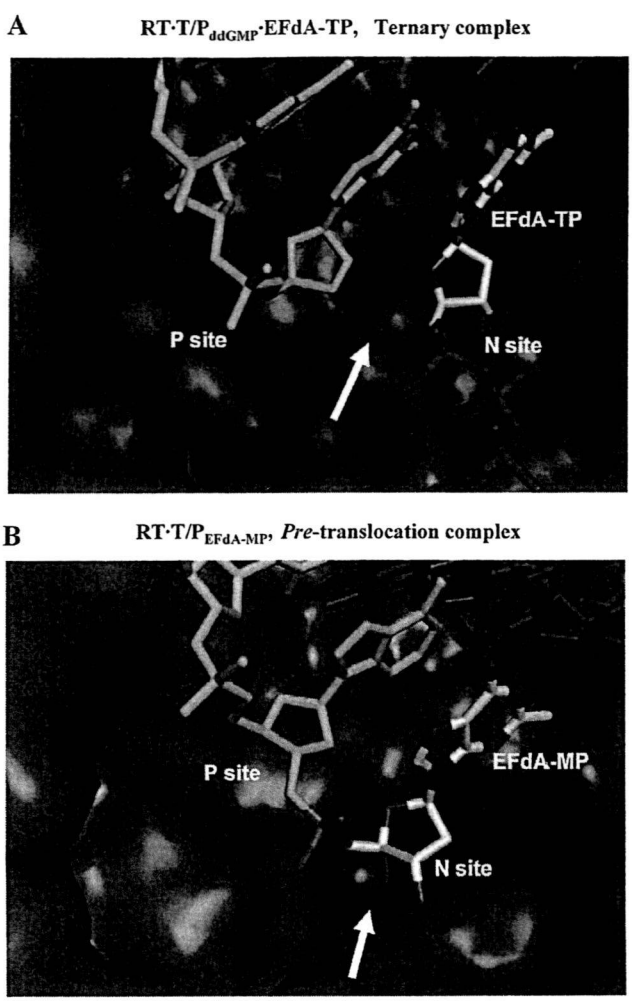

FIGURE 7. **Molecular models representing intermediates of the DNA polymerization reaction.** *A*, molecular model of a ternary complex among RT, DNA, and EFdA-TP. The primer is bound at the P-site, and the incoming EFdA-TP is bound at the N-site. The 4′-ethynyl group of EFdA-TP is bound at a hydrophobic pocket (shown by a *yellow arrow*) defined by residues Met-184, Ala-114, Tyr-115, and Phe-160 and the aliphatic chain of Asp-185. For purposes of clarity the p66 fingers subdomain is not shown. *B*, molecular model of RT bound to EFdA-MP-terminated T/P immediately after incorporation of the inhibitor at the primer terminus and before translocation. The EFdA-MP of the 3′-primer terminus is positioned at the N-site. *C*, schematic representation of RT inhibition by EFdA. After incorporation of EFdA-MP at the 3′-primer terminus RT remains bound to T/P$_{EFdA}$ mostly in a pre-translocation binding mode (*top*). In that binding mode the EFdA-MP at the 3′-primer terminus blocks binding of the incoming dNTP, thus inhibiting DNA polymerization.

the pre-translocation state (Fig. 7*B*). Hence, the stabilization of the primer 3′-terminal EFdA-MP in the pre-translocation state helps it to remain in a position antagonistic to further nucleotide addition and to inhibit DNA polymerization (Fig. 7*C*).

We have observed that in one instance RT stopped not only at the point of EFdA incorporation but also at the position following (Fig. 2*A*, positions *6* and *7*, respectively). Interestingly, we found that RT has enhanced translocation efficiency at this site, both on T/P$_{EFdA-MP}$ and on T/P$_{ddAMP}$ (data not shown). It appears that some translocated T/P$_{EFdA-MP}$ is also elongated by an additional nucleotide. Further polymerization may be inhibited by unfavorable interactions between the 4′-ethynyl group in the elongated template/primer (T/P$_{EFdA-MP-dNMP}$) with protein residues upstream in the DNA-binding cleft. The effect of template on the inhibition mechanism by EFdA is the subject of an ongoing investigation.

RT-catalyzed phosphorolytic excision of chain-terminating NRTIs is a major mechanism of HIV-1 resistance to the nucleoside analog class of therapeutics (26–28, 33). Our previous studies have shown that the NRTI phosphorolytic excision reaction is favored when the primer 3′-terminal nucleotide is in the pre-translocation or N-site (19, 34). The preference of the primer 3′-terminal EFdA-MP to remain in this site suggests that terminal EFdA-MP should undergo facile phosphorolytic removal. EFdA-MP was subject to excision by pyrophosphorolysis somehow faster than ddAMP, which tends to localize in the post-translocation site when at the 3′ terminus of the primer (see Fig. 5*A*). Although EFdA-MP can undergo excision, this process is not overly efficient, apparently because once the nucleotide is excised through pyrophosphorolysis to form EFdA-TP, the latter is rapidly reincorporated. These findings suggest that phosphorolysis may not play a significant role in HIV-1 resistance to EFdA, consistent with the relatively small loss of antiviral potency of EFdA against excision-enhanced HIV-1-containing mutations associated with resistance to AZT (13).

The importance of the 3′-OH in antiviral activity of EFdA is perhaps best highlighted by the observation that EFdA is 10,000-fold more potent at inhibiting HIV-1 replication in PBMCs than is the identical nucleoside lacking a 3′-OH, namely EFddA (Table 2). The 3′-OH on EFdA appears to play a number of roles in contributing to the exceptional antiviral potency of the compound. The 3′-OH on natural dNTP substrates contributes to the efficiency with which RT uses these substrates, and in general NRTIs that lack a 3′-OH are used less efficiently by RT than the base-analogous dNTP (35) (Table 3). Our *in vitro* biochemical data demonstrate that EFdA-TP is approximately 1 and 2 orders of magnitude more potent an inhibitor of RT-catalyzed DNA synthesis *in vitro* than are the

adenine-based NRTIs ddATP and TFV-DP, respectively (Fig. 1*D*), neither of which has a 3′-OH. Indeed, it appears that under identical conditions, RT is at least twice as likely to use EFdA-TP as a substrate over the natural nucleotide dATP (Table 3). This suggests that during HIV-1 reverse transcription, EFdA-TP might be preferentially incorporated, thereby leading to early and profound chain termination and contributing to the observed potent antiviral activity of this nucleoside analog.

NRTIs are administered therapeutically as prodrugs; these must undergo phosphorylation in target cells in order to exert their antiviral activity. The lack of a 3′-OH on current clinically used NRTIs can reduce recognition by cellular nucleoside/nucleotide kinases that have evolved to interact with the 3′-OH present in their natural nucleoside substrates (9). Preliminary studies suggest that EFdA appears to undergo rapid and facile intracellular conversion to the active antiviral EFdA-TP (36), showing that the 4′-ethynyl group does not interfere with recognition by cellular nucleoside/nucleotide kinases. Furthermore, the presence of fluorine at position 2 of the adenine base of EFdA helps to stabilize intracellular levels of EFdA and its phosphorylated products by hindering adenosine deaminase-catalyzed degradation of the molecule (13). Thus, both the 2-fluoro and the 3′-OH of EFdA may contribute to the intracellular accumulation of the antiviral EFdA-TP, thereby leading to its pronounced antiviral activity. We are presently carrying out detailed studies of the intracellular pharmacokinetics of EFdA in comparison with other NRTIs to better understand the dynamics of EFdA phosphorylation and turnover as contributors to the exceptional potency and persistence of its antiviral activity.

Other nucleoside analog inhibitors of HIV-1 RT that possess a 3′-OH have been described (21, 37–42), although these have mechanisms of action quite distinct from that of EFdA. North-methanocarba-2′-deoxyadenosine triphosphate and North-methanocarba-2′-thymidine triphosphate inhibit HIV-1 RT *in vitro* by a mechanism of delayed chain termination, where RT-catalyzed DNA synthesis pauses after the addition of several nucleotides following incorporation of the inhibitor (38, 39). Neither of these compounds has antiviral activity, presumably because of poor intracellular phosphorylation. Entecavir is a nucleoside analog with a 3′-OH that is approved for treatment of hepatitis B infection. Entecavir-TP also has been shown to inhibit HIV-1 RT-catalyzed DNA synthesis by a mechanism of delayed chain termination (40). Entecavir has only weak antiviral activity against HIV-1.

Additionally, nucleoside analogs substituted at the 4′-position have also been described previously (43–46). For example, 4′-azidothymidine and 4′-azidoadenosine both inhibit HIV-1 replication (46) although with potencies 200–2000-fold less than that of EFdA. Both 4′-azido nucleosides also have poor *in vitro* selectivity indices because of significant cytotoxicity. Azidothymidine-TP was shown to inhibit RT-catalyzed DNA synthesis by a type of delayed chain termination; incorporation of two sequential azidothymidine-MP molecules blocked DNA synthesis (44, 45). 4′-Methyl thymidine and 4′-ethyl thymidine both seem to cause pauses and stops in DNA synthesis at the point of incorporation (39). However, neither of these compounds has antiviral activity, because they cannot be phosphorylated by cellular nucleoside kinases. An analog of d4T that has a 4′-ethynyl substitution (Ed4T) is ~10 times more active than the parent compound (47, 48). Because Ed4T lacks a 3′-OH, it inhibits RT as a conventional chain terminator. Interestingly, Ed4T is a better substrate than d4T for phosphorylation by human thymidine kinase 1 (47–50), a property that leads to its increased antiviral potency compared with d4T. The antiviral activity of Ed4T is ~50-fold lower than that of EFdA.

In summary, EFdA is a TDRTI with two functionalities lacking in current therapeutic NRTIs, namely a 4′-ethynyl group and a 3′-OH. These additional properties impart superior antiviral activity to the compound and contribute to its mechanism of action, namely inhibition of primer translocation following EFdA-MP incorporation. This mechanism allows EFdA to act mainly as a *de facto* chain terminator of RT-catalyzed DNA synthesis, despite the presence of a 3′-OH. The present study validates RT nucleic acid translocation as a potential therapeutic target.

REFERENCES

1. Hammer, S. M., Saag, M. S., Schechter, M., Montaner, J. S., Schooley, R. T., Jacobsen, D. M., Thompson, M. A., Carpenter, C. C., Fischl, M. A., Gazzard, B. G., Gatell, J. M., Hirsch, M. S., Katzenstein, D. A., Richman, D. D., Vella, S., Yeni, P. G., and Volberding, P. A. (2006) *Top. HIV Med.* **14,** 827–843
2. Schinazi, R. F., Hernandez-Santiago, B. I., and Hurwitz, S. J. (2006) *Antiviral Res.* **71,** 322–334
3. Parniak, M. A., and Sluis-Cremer, N. (2000) *Adv. Pharmacol.* **49,** 67–109
4. De Clercq, E. (2007) *Verh. K. Acad. Geneeskd. Belg.* **69,** 81–104
5. Sluis-Cremer, N., and Tachedjian, G. (2008) *Virus Res.* **134,** 147–156
6. Deval, J. (2009) *Drugs* **69,** 151–166
7. Sharma, P. L., Nurpeisov, V., Hernandez-Santiago, B., Beltran, T., and Schinazi, R. F. (2004) *Curr. Top. Med. Chem.* **4,** 895–919
8. Sarafianos, S. G., Marchand, B., Das, K., Himmel, D. M., Parniak, M. A., Hughes, S. H., and Arnold, E. (2009) *J. Mol. Biol.* **385,** 693–713
9. Gallois-Montbrun, S., Schneider, B., Chen, Y., Giacomoni-Fernandes, V., Mulard, L., Morera, S., Janin, J., Deville-Bonne, D., and Veron, M. (2002) *J. Biol. Chem.* **277,** 39953–39959
10. Kodama, E. I., Kohgo, S., Kitano, K., Machida, H., Gatanaga, H., Shigeta, S., Matsuoka, M., Ohrui, H., and Mitsuya, H. (2001) *Antimicrob. Agents Chemother.* **45,** 1539–1546
11. Ohrui, H., and Mitsuya, H. (2001) *Curr. Drug Targets Infect. Disord.* **1,** 1–10
12. Ohrui, H., Kohgo, S., Hayakawa, H., Kodama, E., Matsuoka, M., Nakata, T., and Mitsuya, H. (2006) *Nucleic Acids Symp. Ser. (Oxf.) 2006,* 1–2
13. Kawamoto, A., Kodama, E., Sarafianos, S. G., Sakagami, Y., Kohgo, S., Kitano, K., Ashida, N., Iwai, Y., Hayakawa, H., Nakata, H., Mitsuya, H., Arnold, E., and Matsuoka, M. (2008) *Int. J. Biochem. Cell Biol.* **40,** 2410–2420
14. White, K. L., Chen, J. M., Feng, J. Y., Margot, N. A., Ly, J. K., Ray, A. S., Macarthur, H. L., McDermott, M. J., Swaminathan, S., and Miller, M. D. (2006) *Antivir. Ther.* **11,** 155–163
15. Mascolini, M., Larder, B. A., Boucher, C. A., Richman, D. D., and Mellors, J. W. (2008) *Antivir. Ther.* **13,** 1097–1113
16. Le Grice, S. F., and Grüninger-Leitch, F. (1990) *Eur. J. Biochem.* **187,** 307–314
17. Meyer, P. R., Matsuura, S. E., So, A. G., and Scott, W. A. (1998) *Proc. Natl. Acad. Sci. U.S.A.* **95,** 13471–13476
18. Bøyum, A., Løvhaug, D., Tresland, L., and Nordlie, E. M. (1991) *Scand. J. Immunol.* **34,** 697–712
19. Marchand, B., and Götte, M. (2003) *J. Biol. Chem.* **278,** 35362–35372
20. Biaglow, J. E., and Kachur, A. V. (1997) *Radiat. Res.* **148,** 181–187
21. Siddiqui, M. A., Hughes, S. H., Boyer, P. L., Mitsuya, H., Van, Q. N., George, C., Sarafinanos, S. G., and Marquez, V. E. (2004) *J. Med. Chem.* **47,** 5041–5048

22. Stewart, J. J. P. (1989) *J. Comput. Chem.* **10,** 209–220
23. Hattori, S., Ide, K., Nakata, H., Harada, H., Suzu, S., Ashida, N., Kohgo, S., Hayakawa, H., Mitsuya, H., and Okada, S. (2009) *Antimicrob. Agents Chemother.* **53,** 3887–3893
24. Quan, Y., Liang, C., Inouye, P., and Wainberg, M. A. (1998) *Nucleic Acids Res.* **26,** 5692–5698
25. Tong, W., Lu, C. D., Sharma, S. K., Matsuura, S., So, A. G., and Scott, W. A. (1997) *Biochemistry* **36,** 5749–5757
26. Sluis-Cremer, N., Arion, D., and Parniak, M. A. (2000) *Cell. Mol. Life Sci.* **57,** 1408–1422
27. Arion, D., Kaushik, N., McCormick, S., Borkow, G., and Parniak, M. A. (1998) *Biochemistry* **37,** 15908–15917
28. Meyer, P. R., Matsuura, S. E., Mian, A. M., So, A. G., and Scott, W. A. (1999) *Mol. Cell* **4,** 35–43
29. Sarafianos, S. G., Clark, A. D., Jr., Das, K., Tuske, S., Birktoft, J. J., Ilankumaran, P., Ramesha, A. R., Sayer, J. M., Jerina, D. M., Boyer, P. L., Hughes, S. H., and Arnold, E. (2002) *EMBO J.* **21,** 6614–6624
30. Sarafianos, S. G., Clark, A. D., Jr., Tuske, S., Squire, C. J., Das, K., Sheng, D., Ilankumaran, P., Ramesha, A. R., Kroth, H., Sayer, J. M., Jerina, D. M., Boyer, P. L., Hughes, S. H., and Arnold, E. (2003) *J. Biol. Chem.* **278,** 16280–16288
31. Tuske, S., Sarafianos, S. G., Clark, A. D., Jr., Ding, J., Naeger, L. K., White, K. L., Miller, M. D., Gibbs, C. S., Boyer, P. L., Clark, P., Wang, G., Gaffney, B. L., Jones, R. A., Jerina, D. M., Hughes, S. H., and Arnold, E. (2004) *Nat. Struct. Mol. Biol.* **11,** 469–474
32. Yang, G., Wang, J., Cheng, Y., Dutschman, G. E., Tanaka, H., Baba, M., and Cheng, Y. C. (2008) *Antimicrob. Agents Chemother.* **52,** 2035–2042
33. Sluis-Cremer, N., Arion, D., Parikh, U., Koontz, D., Schinazi, R. F., Mellors, J. W., and Parniak, M. A. (2005) *J. Biol. Chem.* **280,** 29047–29052
34. Marchand, B., White, K. L., Ly, J. K., Margot, N. A., Wang, R., McDermott, M., Miller, M. D., and Götte, M. (2007) *Antimicrob. Agents Chemother.* **51,** 2911–2919
35. Feng, J. Y., Murakami, E., Zorca, S. M., Johnson, A. A., Johnson, K. A., Schinazi, R. F., Furman, P. A., and Anderson, K. S. (2004) *Antimicrob. Agents Chemother.* **48,** 1300–1306
36. Nakata, H., Amano, M., Koh, Y., Kodama, E., Yang, G., Bailey, C. M., Kohgo, S., Hayakawa, H., Matsuoka, M., Anderson, K. S., Cheng, Y. C., and Mitsuya, H. (2007) *Antimicrob. Agents Chemother.* **51,** 2701–2708
37. Strerath, M., Cramer, J., Restle, T., and Marx, A. (2002) *J. Am. Chem. Soc.* **124,** 11230–11231
38. Boyer, P. L., Julias, J. G., Marquez, V. E., and Hughes, S. H. (2005) *J. Mol. Biol.* **345,** 441–450
39. Boyer, P. L., Julias, J. G., Ambrose, Z., Siddiqui, M. A., Marquez, V. E., and Hughes, S. H. (2007) *J. Mol. Biol.* **371,** 873–882
40. Tchesnokov, E. P., Obikhod, A., Schinazi, R. F., and Götte, M. (2008) *J. Biol. Chem.* **283,** 34218–34228
41. Summerer, D., and Marx, A. (2005) *Bioorg. Med. Chem. Lett.* **15,** 869–871
42. Di Pasquale, F., Fischer, D., Grohmann, D., Restle, T., Geyer, A., and Marx, A. (2008) *J. Am. Chem. Soc.* **130,** 10748–10757
43. Maag, H., Rydzewski, R. M., McRoberts, M. J., Crawford-Ruth, D., Verheyden, J. P., and Prisbe, E. J. (1992) *J. Med. Chem.* **35,** 1440–1451
44. Chen, M. S., Suttmann, R. T., Papp, E., Cannon, P. D., McRoberts, M. J., Bach, C., Copeland, W. C., and Wang, T. S. (1993) *Biochemistry* **32,** 6002–6010
45. Chen, M. S., Suttmann, R. T., Wu, J. C., and Prisbe, E. J. (1992) *J. Biol. Chem.* **267,** 257–260
46. Maag, H., Nelson, J. T., Steiner, J. L., and Prisbe, E. J. (1994) *J. Med. Chem.* **37,** 431–438
47. Nitanda, T., Wang, X., Kumamoto, H., Haraguchi, K., Tanaka, H., Cheng, Y. C., and Baba, M. (2005) *Antimicrob. Agents Chemother.* **49,** 3355–3360
48. Tanaka, H., Haraguchi, K., Kumamoto, H., Baba, M., and Cheng, Y. C. (2005) *Antivir. Chem. Chemother.* **16,** 217–221
49. Hsu, C. H., Hu, R., Dutschman, G. E., Yang, G., Krishnan, P., Tanaka, H., Baba, M., and Cheng, Y. C. (2007) *Antimicrob. Agents Chemother.* **51,** 1687–1693
50. Yang, G., Dutschman, G. E., Wang, C. J., Tanaka, H., Baba, M., Anderson, K. S., and Cheng, Y. C. (2007) *Antiviral Res.* **73,** 185–191

JOURNAL OF VIROLOGY, Apr. 2009, p. 3059–3068 Vol. 83, No. 7
0022-538X/09/$08.00+0 doi:10.1128/JVI.02539-08

Non-Cleavage Site Gag Mutations in Amprenavir-Resistant Human Immunodeficiency Virus Type 1 (HIV-1) Predispose HIV-1 to Rapid Acquisition of Amprenavir Resistance but Delay Development of Resistance to Other Protease Inhibitors▽

Manabu Aoki,[1,2] David J. Venzon,[3] Yasuhiro Koh,[1] Hiromi Aoki-Ogata,[1] Toshikazu Miyakawa,[1] Kazuhisa Yoshimura,[1] Kenji Maeda,[1,4] and Hiroaki Mitsuya[1,4]*

Departments of Hematology and Infectious Diseases, Kumamoto University Graduate School of Medical and Pharmaceutical Sciences, Kumamoto 860-8556, Japan[1]; Institute of Health Sciences, Kumamoto Health Science University, Kumamoto 861-5598, Japan[2]; and Biostatistics and Data Management Section[3] and Experimental Retrovirology Section, HIV and AIDS Malignancy Branch,[4] Center for Cancer Research, National Cancer Institute, National Institutes of Health, Bethesda, Maryland 20892

Received 10 December 2008/Accepted 20 January 2009

In an attempt to determine whether mutations in Gag in human immunodeficiency virus type 1 (HIV-1) variants selected with a protease inhibitor (PI) affect the development of resistance to the same or a different PI(s), we generated multiple infectious HIV-1 clones carrying mutated Gag and/or mutated protease proteins that were identified in amprenavir (APV)-selected HIV-1 variants and examined their virological characteristics. In an HIV-1 preparation selected with APV (33 passages, yielding HIV_{APVp33}), we identified six mutations in protease and six apparently critical mutations at cleavage and non-cleavage sites in Gag. An infectious recombinant clone carrying the six protease mutations but no Gag mutations failed to replicate, indicating that the Gag mutations were required for the replication of HIV_{APVp33}. An infectious recombinant clone that carried wild-type protease and a set of five Gag mutations ($rHIV_{WTpro}^{12/75/219/390/409gag}$) replicated comparably to wild-type HIV-1; however, when exposed to APV, $rHIV_{WTpro}^{12/75/219/390/409gag}$ rapidly acquired APV resistance. In contrast, the five Gag mutations significantly delayed the acquisition of HIV-1 resistance to ritonavir and nelfinavir (NFV). Recombinant HIV-1 clones containing NFV resistance-associated mutations, such as D30N and N88S, had increased susceptibilities to APV, suggesting that antiretroviral regimens including both APV and NFV may bring about favorable antiviral efficacy. The present data suggest that the preexistence of certain Gag mutations related to PI resistance can accelerate the emergence of resistance to the PI and delay the acquisition of HIV resistance to other PIs, and these findings should have clinical relevance in the therapy of HIV-1 infection with PI-including regimens.

Combination antiretroviral therapy using reverse transcriptase inhibitors and protease inhibitors (PIs) produces substantial suppression of viral replication in human immunodeficiency virus type 1 (HIV-1)-infected patients (3, 27, 28, 42). However, the emergence of drug-resistant HIV-1 variants in such patients has limited the efficacy of combination chemotherapy. HIV-1 variants resistant to all of the currently available antiretroviral therapeutics have emerged both in vitro and in vivo (6, 16, 27, 30). Of note, a number of PI resistance-associated amino acid substitutions in the active site of protease have been identified, and such substitutions have considerable impact on the catalytic activity of protease. This impact is reflected by impaired processing of Gag precursors in mutated-protease-carrying virions and by decreased catalytic efficiency of the protease toward peptides with natural cleavage sites (7, 29, 31, 43).

However, the highly PI-resistant viruses frequently have amino acid substitutions at the p7-p1 and p1-p6 cleavage sites in Gag. These mutations have been identified in PI-resistant HIV-1 variants selected in vitro (2, 5, 8, 29) and in HIV-1 isolated from patients with AIDS for whom chemotherapy including PIs was failing (26, 40, 47, 48). These mutations are known to compensate for the enzymatic impairment of protease, per se, resulting from the acquisition of PI resistance-conferring mutations within the protease-encoding region. Moreover, certain mutations at non-cleavage sites in Gag have been shown previously to be essential for the replication of HIV-1 variants in the presence of PIs (14, 15). Although a few amino acid substitutions at cleavage and non-cleavage sites in Gag have been shown to be associated with resistance to PIs, the roles and impact of amino acid substitutions in Gag for the HIV-1 acquisition of PI resistance remain to be elucidated.

In the present study, we identified novel Gag non-cleavage site mutations in addition to multiple mutations in the protease gene during in vitro selection of HIV-1 variants highly resistant to amprenavir (APV). We show that the non-cleavage site mutations were important for not only the replication of the mutated-protease-carrying HIV-1 but also the accelerated acquisition of HIV-1 resistance to APV and an unrelated PI, nelfinavir (NFV). We also show that recombinant HIV-1 clones containing NFV resistance-associated mutations, such

* Corresponding author. Mailing address: Department of Hematology, Kumamoto University School of Medicine, 1-1-1 Honjo, Kumamoto 860-8556, Japan. Phone: (81) 96-373-5156. Fax: (81) 96-363-5265. E-mail: hm21q@nih.gov.

▽ Published ahead of print on 28 January 2009.

as D30N and N88S, had increased susceptibility to APV, suggesting that antiretroviral regimens including both APV and NFV may bring about favorable antiviral efficacy.

MATERIALS AND METHODS

Cells and antiviral agents. MT-2 and MT-4 cells were grown in RPMI 1640-based culture medium, and 293T cells were propagated in Dulbecco's modified Eagle's medium. These media were supplemented with 10% fetal calf serum (HyClone, Logan, UT), 50 U/ml penicillin, and 50 μg/ml streptomycin. APV was kindly provided by GlaxoSmithKline, Research Triangle Park, NC. Saquinavir (SQV) and ritonavir (RTV) were provided by Roche Products Ltd. (Welwyn Garden City, United Kingdom) and Abbott Laboratories (Abbott Park, IL), respectively. NFV and indinavir (IDV) were kindly provided by Japan Energy Inc., Tokyo.

Generation of PI-resistant HIV-1 in vitro. For the generation of PI-resistant HIV-1, various PI-resistant HIV-1 strains were propagated in the presence of increasing concentrations of a drug in a cell-free fashion as described previously (44, 45). In brief, on the first passage, MT-2 or MT-4 cells (5×10^5) were exposed to 500 50% tissue culture infective doses ($TCID_{50}$) of each infectious molecular HIV-1 clone and cultured in the presence of various PIs at initial concentrations of 0.01 to 0.06 μM. On the last day of each passage (approximately day 7), 1 ml of the cell-free supernatant was harvested and transferred to a culture of fresh uninfected cells in the presence of increased concentrations of the drug for the following round of culture. In this round of culture, three drug concentrations (increased by one-, two-, and threefold compared to the previous concentration) were employed. When the replication of HIV-1 in the culture was confirmed by substantial Gag protein production (greater than 200 ng/ml), the highest drug concentration among the three concentrations was used to continue the selection (for the next round of culture). This protocol was repetitively used until the drug concentration reached the targeted concentration. Proviral DNA from the lysates of infected cells at various passages was subjected to nucleotide sequencing.

Determination of nucleotide sequences. Molecular cloning and the determination of nucleotide sequences of HIV-1 passaged in the presence of each PI were performed as described previously (44, 45). In brief, high-molecular-weight DNA was extracted from HIV-1-infected MT-2 and MT-4 cells by using the InstaGene matrix (Bio-Rad Laboratories, Hercules, CA) and was subjected to molecular cloning, followed by sequence determination. The primers used for the first-round PCR amplification of the entire Gag- and protease-encoding regions of the HIV-1 genome were LTR F1 (5'-GAT GCT ACA TAT AAG CAG CTG C-3') and PR12 (5'-CTC GTG ACA AAT TTC TAC TAA TGC-3'). The first-round PCR mixture consisted of 5 μl of proviral DNA solution, 2.0 U of premix *Taq* (Ex *Taq* version; Takara Bio Inc., Otsu, Japan), and 12.5 pmol of each of the first-round PCR primers in a total volume of 50 μl. The PCR conditions used were an initial 2-min step at 94°C, followed by 30 cycles of 30 s at 94°C, 30 s at 58°C, and 3 min at 72°C, with a final 8 min of extension at 72°C. The first-round PCR products (1 μl) were used directly in the second round of PCR with primers LTR F2 (5'-GAG ACT CTG GTA ACT AGA GAT C-3') and Ksma2.1 (5'-CCA TCC CGG GCT TTA ATT TTA CTG GTA C-3') under the same PCR conditions described above. The second-round PCR products were purified with spin columns (MicroSpin S-400 HR; Amersham Biosciences Corp., Piscataway, NJ), cloned directly, and subjected to sequencing with a model 377 automated DNA sequencer (Applied Biosystems, Foster City, CA).

Generation of recombinant HIV-1 clones. The PCR products obtained as described above were digested with two of the three enzymes BssHII, ApaI, and SmaI, and the obtained fragments were introduced into pHIV-1_{NLSma}, designed to have a SmaI site by changing two nucleotides (2590 and 2593) of pHIV-1_{NL4-3} (15, 19). To generate HIV-1 clones carrying the mutations, site-directed mutagenesis using the QuikChange site-directed mutagenesis kit (Stratagene, La Jolla, CA) was performed, and the mutation-containing genomic fragments were introduced into pHIV-1_{NLSma}. Determination of the nucleotide sequences of plasmids confirmed that each clone had the desired mutations but no unintended mutations. 293T cells were transfected with each recombinant plasmid by using Lipofectamine 2000 reagent (Invitrogen, Carlsbad, CA), and the thus-obtained infectious virions were harvested 48 h after transfection and stored at −80°C until use.

Drug sensitivity assays. Assays for HIV-1 p24 Gag protein production were performed with MT-4 cells as described previously (1, 20, 24). In brief, MT-4 cells (10^5/ml) were exposed to 100 $TCID_{50}$ of infectious molecular HIV-1 clones in the presence or absence of various concentrations of drugs and were incubated at 37°C. On day 7 of culture, the supernatant was harvested and the amounts of p24 Gag protein were determined by using a fully automated chemiluminescent enzyme immunoassay system (Lumipulse F; Fujirebio Inc., Tokyo). The drug concentrations that suppressed the production of p24 Gag protein by 50% (50% inhibitory concentrations [IC_{50}]) were determined by comparing the levels of p24 production with that in a drug-free control cell culture. All assays were performed in triplicate.

Replication kinetic assay. MT-2 or MT-4 cells (10^5) were exposed to each infectious HIV-1 clone (5 ng of p24 Gag protein/ml) for 3 h, washed twice with phosphate-buffered saline, and cultured in 10 ml of complete medium as described previously (1, 14). Culture supernatants (50 μl) were harvested every other day, and the p24 Gag amounts were determined as described above.

CHRA. Two titrated infectious clones to be compared for their replicative capabilities or fitness in the competitive HIV-1 replication assay (CHRA) were combined and added to freshly prepared MT-4 cells (2×10^5) in the presence or absence of various concentrations of PIs as described previously (21, 36). Briefly, a fixed amount (200 $TCID_{50}$) of one infectious clone was combined with three different amounts (100, 200, and 300 $TCID_{50}$) of the other infectious clone, and the mixture was added to the culture of MT-4 cells. On the following day, one-third of infected MT-4 cells were harvested and washed twice with phosphate-buffered saline, and cellular DNA was extracted and subjected to nested PCR and sequencing as described above. The HIV-1 coculture that best approximated a 50:50 mixture on day 1 was further propagated, and the remaining cultures were discarded. Every 7 days, the cell-free supernatant of the virus coculture was transmitted to fresh uninfected MT-4 cells. The cells harvested at the end of each passage were subjected to direct DNA sequencing, and viral population changes were determined. The persistence of the original amino acid substitutions was confirmed for all infectious clones used in this assay.

Statistical analysis of selection profiles of infectious HIV-1 clones. The selection profiles of various infectious HIV-1 clones were compared as follows. The logarithms of the concentrations were modeled as normally distributed variables with possible left censoring. The mean was assumed to be a quadratic function of the passage number. The difference between two curves was assessed by combining the estimated covariance-weighted differences of the linear and quadratic coefficients and comparing the result to computer simulations for the same quantity generated under the specific null hypothesis for that difference. SAS 9.1.3 (SAS Institute, Cary, NC) was used for all the computations. All *P* values are two tailed, and for figures with more than two curves, the values were corrected by the Hochberg method for multiple pairwise comparisons.

RESULTS

Amino acid sequences of Gag and protease of HIV-1 passaged in the presence of APV. A wild-type HIV-1 strain (HIV_{WT}) was propagated in MT-2 cells in the presence of increasing concentrations of APV, and the proviral DNA sequences in those MT-2 cells were determined at passages 3, 12, and 33 (Fig. 1). By passage 3, when HIV-1 was propagating in the presence of 0.04 μM APV (yielding HIV_{APVp3}), no amino acid substitutions in protease were identified but 5 of 10 clones had acquired the substitution of arginine for leucine at position 75 (L75R) in Gag. By passage 12 (at 0.18 μM APV), two APV-related resistance mutations (L10F and M46L) in protease had emerged and one mutation (H219Q) in Gag had been added. By passage 33 (at 10 μM; yielding HIV_{APVp33}), six APV-related amino acid substitutions, one primary mutation (I84V) and five secondary mutations (L10F, V32I, M46I, I54M, and A71V), in protease had emerged (Fig. 1A). In addition, a p1-p6 cleavage site mutation in Gag (L449F) was identified in all 10 HIV-1 clones of HIV_{APVp33} examined, and five non-cleavage site mutations (E12K, L75R, H219Q, V390D, and R409K) were seen in Gag of HIV_{APVp33} (Fig. 1B). Cleavage site mutations have been known to emerge when amino acid substitutions in protease are accumulated and HIV-1 develops resistance to PIs both in vitro and in vivo (5, 8). Intriguingly, the present data suggest that certain amino acid substitutions in non-cleavage sites of Gag (i.e., L75R and

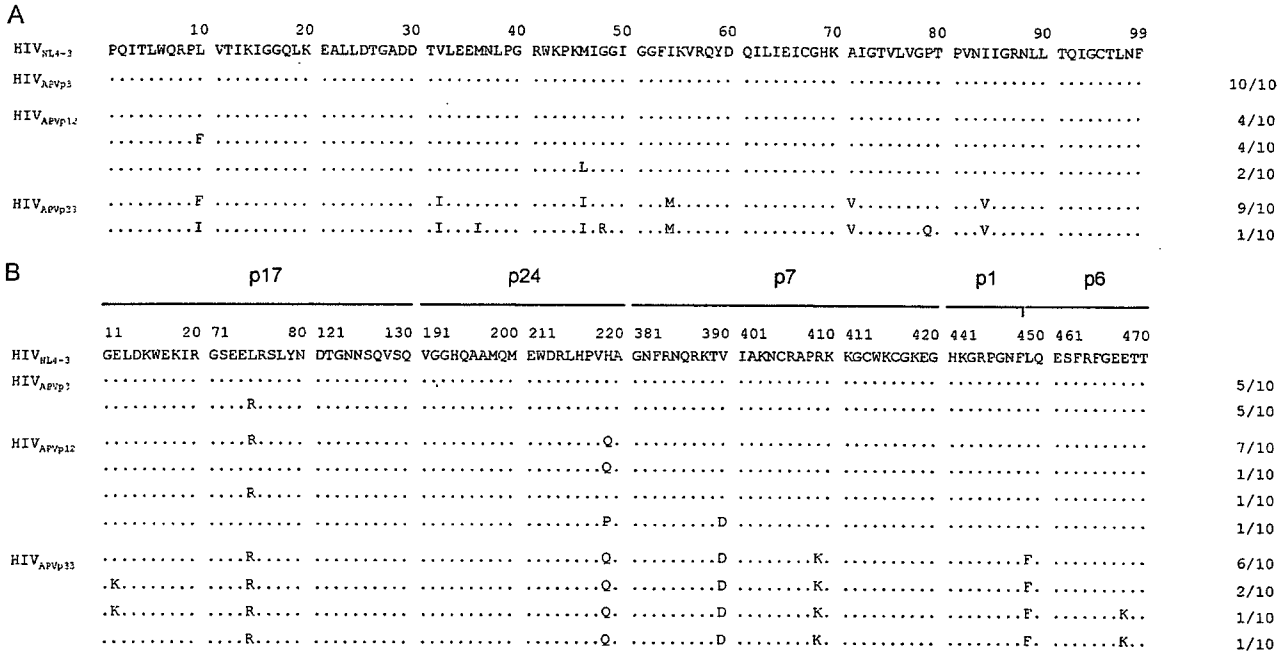

FIG. 1. Amino acid sequences deduced from the nucleotide sequences of protease (A)- and Gag (B)-encoding regions of proviral DNA isolated at the indicated passages (p3, p12, and p33) from HIV-1_{NL4-3} variants selected in the presence of APV. The amino acid sequences of the protease and Gag proteins of wild-type HIV-1_{NL4-3} are shown at the top as a reference. Identity to the sequence at individual amino acid positions is indicated by dots. The numbers of clones with the given amino acid substitutions among a total of 10 clones are listed.

H219Q) may emerge earlier and in greater numbers than amino acid substitutions in protease, at least in the case of HIV-1 selection with APV. The amino acid substitutions that emerged in the virus and the pattern and order of such substitutions were largely in agreement with the data in the previous report by Gatanaga et al. (15). The present results suggested that the non-cleavage site mutations observed may play a key role in the development of HIV-1 resistance against PIs and that especially the two Gag mutations H219Q and R409K may be required for the development of PI resistance.

Mutations in Gag are required for the replication of HIV$_{APVp33}$. In order to examine the effects of the mutations identified in Gag as described above on the replication profile of HIV-1, we generated infectious recombinant HIV-1 clones containing the six mutations (L10F, V32I, M46I, I54V, A71V, and I84V) in protease seen in HIV$_{APVp33}$. A recombinant HIV-1 clone containing the protease of HIV$_{APVp33}$ plus a wild-type Gag (rHIV$_{APVp33pro}^{WTgag}$) or the L449F cleavage site mutation-containing Gag (rHIV$_{APVp33pro}^{449gag}$) failed to replicate in MT-2 cells over the 7-day period of culture (Fig. 2A), indicating that these Gag species do not support the growth of HIV$_{APVp33}$. Therefore, we next generated a recombinant HIV-1 clone containing the protease of HIV$_{APVp33}$ and the Gag protein with the five non-cleavage site mutations (E12K, L75R, H219Q, V390D, and R409K; rHIV$_{APVp33pro}^{12/75/219/390/409gag}$), which replicated moderately under the same conditions (Fig. 2A). The addition of the cleavage site mutation L449F, generating rHIV$_{APVp33pro}^{12/75/219/390/409/449gag}$, further improved the replication of the virus. In MT-4 cells, in which HIV-1 generally replicates more quickly and efficiently than in MT-2 cells, rHIV$_{APVp33pro}^{WTgag}$ and rHIV$_{APVp33pro}^{449gag}$ replicated moderately; however, both rHIV$_{APVp33pro}^{12/75/219/390/409gag}$ and rHIV$_{APVp33pro}^{12/75/219/390/409/449gag}$ replicated comparably to HIV$_{WT}$ (Fig. 2B), due presumably to the greater replication of HIV-1 in MT-4 cells, making the difference relatively indistinct. These data clearly indicate that both non-cleavage site and cleavage site mutations in Gag contribute to the robust fitness of HIV$_{APVp33}$. We also attempted to examine the effects of combined Gag mutations on the replication of HIV-1 containing wild-type protease and generated three recombinant HIV clones, rHIV$_{WTpro}^{75/219gag}$, rHIV$_{WTpro}^{219/409gag}$, and rHIV$_{WTpro}^{12/75/219/390/409gag}$. The replication rates of these three recombinant clones turned out to be comparable to that of HIV$_{WT}$ when examined in MT-2 and MT-4 cells (Fig. 2C and D), unlike the finding by Doyon and his colleagues that the cleavage site mutation L449F compromised the replication of HIV-1 containing wild-type protease (8).

Gag mutations predispose HIV-1 to rapidly acquire APV resistance. The appearance of two non-cleavage site mutations (L75R and H219Q) in Gag prior to the emergence of mutations in protease (Fig. 1) prompted us to examine whether these two Gag mutations predisposed the virus to the acquisition of APV resistance-associated mutations in protease. We thus attempted to select APV-resistant HIV-1 by propagating HIV$_{NL4-3}$ (HIV$_{WT}$) and rHIV$_{WTpro}^{75/219gag}$ in the presence of increasing concentrations of APV (Fig. 3). When we compared the selection curves of these two viruses, there was no significant difference (P, 0.53 and 0.65 for propagation in MT-2 and MT-4 cells, respectively). We then examined the effects of two mutated Gag species containing two and five mutations (H219Q and R409K and E12K, L75R, H219Q, V390D, and